2014

# Fabrication of Nanoporous Gold and Biological Applications

Badharinadh Uppalapati
*Virginia Commonwealth University*

# Fabrication of Nanoporous Gold and Biological Applications

A dissertation submitted in partial fulfillment of the requirements for the degree of Masters of Science at Virginia Commonwealth University.

by

Badharinadh Uppalapati

Master of Science, Osmania University, India, 2010

Bachelor of Science, Osmania University, India, 2007

Director: Maryanne M. Collinson

Professor, Department of Chemistry

Virginia Commonwealth University

Richmond, Virginia

June, 2014

# Acknowledgment

I am grateful and appreciative for the guidance, and support of my advisor Professor Maryanne M. Collinson. I am thankful to my advisor for providing me an opportunity to work in her research group and for her abundant help and invaluable assistance, through my entire study process. I would like to thank Dr. Rodney Daniels for his help in my project and funding for characterization studies. I would like to thank Dr. Penny Reynolds, Dr. Nicholas Farrell and Division of Animal Research for donation of samples for my study. I would like to thank Dr. Sarah Rutan for her help and support. I would also like to thank Dr. Dmitry Pestov for his instructions and help concerning instrumental analysis. I am thankful to Dr. Logudarai Radhakrishnan and Dr. Leela Srinivas, Dr. Martin Michael Dcona, Dr. Daniel Gerard, K. Durga Prasad for their invaluable support and guidance during the study. I am also thankful to all my lab mates for useful discussions and encouragement during the study. Finally, I am thankful to my parents and friends for their support, guidance and strong encouragement during my graduate study.

# Table of Contents

# List of Figures

# List of Tables

# Abstract

**FABRICATION OF NANOPOROUS GOLD AND BIOLOGICAL APPLICATIONS**

By Badharinadh Uppalapati

A Dissertation submitted in partial fulfillment of the requirements for the degree of Master of Science at Virginia Commonwealth University.

Virginia Commonwealth University, 2014

Major Director: Maryanne M. Collinson,
Professor, Department of Chemistry

Fabrication of nanoporous gold electrodes by dealloying Au:Ag alloys has attracted much attention in sensing applications. In the first part of this work, the electrochemical response of the redox active molecule, potassium ferricyanide, in a solution of bovine serum albumin in buffer, serum or blood was studied using nanoporous gold and comparisons made to planar gold. Nanoporous gold electrodes with different surface areas and porosity were prepared by dealloying Au:Ag alloy in nitric acid for different dealloying times, specifically, 7.5, 10, 12.5, 20 minutes. Characterization was done using scanning electron microscopy (SEM), X-ray

photoelectron spectroscopy (XPS), energy dispersive X-ray spectroscopy (EDX), and cyclic voltammetry (CV).

Using cyclic voltammetry, planar gold electrodes exposed to bovine serum albumin in buffer showed a decrease in Faradaic peak current and an increase in peak splitting for potassium ferricyanide. The time required for the peak Faradaic current to drop to one-half of its original value was 3 minutes. At nanoporous gold electrodes, however, no significant reduction in Faradaic peak current or increase in peak splitting was observed. Nanoporous gold electrodes having the smallest pore size and largest surface area showed ideal results to biofouling. These electrodes are believed to impede the mass transport of large biomolecules while allowing small redox molecules to exchange electrons effectively with the electrode.

In the second part of this work, the open circuit potential (OCP) of biologic solutions (e.g., blood) was measured using nanoporous gold electrodes. Historically, the measurement of blood redox potential has been hindered due to significant fouling and surface passivation of the metal electrodes. As nanoporous gold electrodes retained electrochemical activity of redox probes like potassium ferricyanide in human serum and rabbit blood, they were used to measure the OCP of blood and plasma from various animals like pig, rabbit, rat, monkey and humans. Comparisons were made to planar gold electrodes. The OCP values at both the planar gold and nanoporous gold electrodes were different from each other and there was variability due to different constituents present in blood and plasma. The OCP of rabbit blood and crashed rabbit blood was measured and the values were found to be different from each other

indicating that ORP helps in measuring the animal condition. Ascorbic acid was added to rabbit and sheep blood and OCP measured at the nanoporous electrodes. Addition of reducing agent to blood at different intervals and different concentrations showed a change in potential with concentration.

# Chapter 1: Introduction

## 1.1. Introduction

During the last couple of decades, many biosensor devices have been manufactured, but (to present) many of these devices have had limited success because of their imperfect electrochemical performance in complex biologic solutions. Sensors can fail for many reasons. These reasons can be divided into two classifications, component based failures and biocompatibility issues.[1,2] The latter reason is most applicable in the work described in this thesis and is described below.

A widely known and illustrated phenomenon associated with biological systems is that of protein adsorption, which will take place when a conducting metal is exposed to biologic samples.[1,2] Since the early inception of biological sensors, a wide variety of techniques have been used to understand and scrutinize the behavior of proteins on planar and nanostructured surfaces.[3-5] Of crucial importance for electrochemical biosensors is the direct electron transfer (ET) between an electrode and the various redox species in solution. These biosensors need electrodes that have sensibly fast ET kinetics with various species in solution and are biocompatible and immune to protein adsorption and denaturation. In many situations, significant changes in protein structural and functionality occur due to the contact with uncoated metal surfaces.

Modification of both electrode and protein may be necessary to prevent this from taking place.[3,4,6] The problem connected with many electrochemically-based biosensors is the drifting of signal with time caused either by (i) the biofouling of the outer most surfaces of the sensor or (ii) passivation of the working electrode.

In general, biofouling is the accumulation of microorganisms, plants, algae etc on wetted surfaces. Biofouling on outer surfaces, which generally involves the deposition of proteins and cellular attachment, will create a supplementary solute mass transport hindrance or barrier layer. This layer usually forms over the outer surface of the sensor and can lead to unusual measurements. The adsorption of protein on the metal surface can decrease the sensor response and potentially prejudice the measurement. It is thus imperative that a sensor to be used in blood, for example, must have an interface with adequate level of hemo-compatibility.[5,7] There is a clear need for anti-biofouling coatings for biosensors and medical implants. Biofouling prevents intimate contact between the device and tissue, which has advert effect on measurements.

When the electrode is exposed to biological solution, biological species are accumulated on the surface of the electrode eventually blocking the surface of the electrode results in electrode passivation. Over the years several approaches have been developed to overcome the impact of protein adsorption on the electrochemical activity of redox active molecules at electrode surfaces. One early approach was performed by placement of a polycarbonate microporous membrane on the electrode surface or by coating microporous polycarbonate membranes with diamond-like carbon.[8-10] This improved the sensor response in biofouling solutions.[8-10] Another widespread method

involved chemical modification of the electrode surface with pyridinethiol to enable cytochrome c to efficiently exchange the electrons without concurrent adsorption followed by denaturation.[11] This was also achieved by Natan et al who modified the electrode (i.e, tin oxide) with of 12-nm-diameter colloidal Au particles.[12] The direct electrochemistry of horse heart cytochrome c in solution was achieved in this case as well.

Poly(ethylene glycol) (PEG), or as it is often called poly(ethylene oxide) (PEO), is a polymer that has a considerable importance in biomaterials and many other applications. At the same time, PEG has also been used in biological research as a coagulating agent for proteins and viruses. The reduction of biofouling has been achieved by incorporating on to biomaterials like Vascular grafts, intravascular stents and ligaments. This approach has a tremendous advantage to reduce the biofouling.[13] The use of PEG in biosensors would minimize the signal drift or passivation of an electrode response with time upon the exposure to ascorbic acid in human blood.[13-16] PEG coated gold electrodes have also been used to facilitate the oxidation of ascorbic acid at modified gold electrodes, which in turn was compared with the bare gold electrodes.[16] Perhaps the most popular approach to reduce the effect of biofouling involves polymer coatings on metal surfaces. Several examples of polymeric materials used include polyurethanes-dermatan sulfate,[17] and diamond-like carbon,[8,9] polyethylene glycols or oxides.[13]

One inherent problem with these approaches is that electrode modification can impede electron exchange at the electrode surface and subsequently bias or alter the

results due to selective partitioning of certain analyte species. Furthermore, these methods are not always suitable for many clinical applications.[11,12,20,23] Instead of preventing adsorption using modification of electrode, we have mainly focused on nanostructure of the electrode to minimize the impact of protein adsorption on the redox measurements made in blood.[18] Detailed discussion about preparing nanostructured electrodes and electrochemical response is given in chapter 2, 3.

## 1.2. Nanostructured Metal Electrodes

Nanomaterials have received an enormous interest in the last two decades in the emerging fields such as nanotechnology and nanochemistry. Presently, many researchers are working in the field of nanomaterials due to their exceptional chemical and physical properties such as high specific surface area,[19] high surface–to-volume ratio, strength, and ductility. These properties make nanomaterials ideal for applications in many fields like biosensors, nanoelectronics, microelectromechanical devices, biology, and medicine.[20-23] Some examples of nanomaterials include carbon nanotubes and fullerene from carbon, porous-carbon polymer composites,[21] and nanoporous silicon.[23]

High surface area materials can be prepared using two approaches. The first approach is to prepare small nanosize particles that have high surface-to-volume ratios and the second approach is to generate materials with voids or pores to increase surface area. Porous materials are divided according to their size given by IUPAC nomenclature, macroporous (>5O nm), mesoporous (2-5O nm), microporous (<2 nm)[24]. Although nanoporous gold falls under mesoporous, most researchers term it as nanoporous. In my thesis "nanoporous" is used.

There are different approaches for the fabrication of nanostructured gold electrodes with each having its own distinctive advantages and disadvantages. Macroporous gold electrodes are prepared from mondisperse latex spheres,[25,26] nanoporous gold electrode by dealloying a gold - silver alloy, nanoparticle based gold electrode from gold nanoparticles,[27,28] hierarchical gold electrodes from hierarchical polystryrene latex spheres,[26] nanopillar electrodes by electrodeposition,[29] and nanofiber gold electrodes by electronspun gold.[30] Among the many different types and configurations of nanostructured metals, nanoporous gold with a three-dimensional morphology with small pores in nanometer size and continuous interconnected ligaments, have emerged has important material in electrochemistry.[31] Nanoporous gold has a significantly higher surface area-to-volume ratio compared to planar gold.

### 1.2.1. Nanoporous Gold: Fabrication

Fabrication of nanoporous gold consists of several steps: 1) selection of the alloy and 2) dealloying the alloy.

### 1.2.2. Alloy selection

Alloys have different compositions of different elements. Nanostructure is fomed by dealloying the selected metal in nitric acid

### 1.2.3. Binary alloys

Nanoporous gold can be fabricated by using Au-Ag alloys (most popular) but also Au-Zn[32], Au-Al,[33] or Au-Ni.[34] Nanoporous structured gold can be prepared by dealloying Au-Zn in ionic liquid [32] or the Au-Ag alloys in nitric acid.[35] Au-Ni alloy film was synthesized and then electrochemical dealloying under potential control in stronger

acids like sulfuric acid and perchloric acid.[34] Nanoporous gold can also be fabricated by taking different compositions of Gold-Aluminium alloys for example, Au(20)/Al(80), Au(30)/Al(70).[36,37] and dealloying by Ag(50)/Au(50). Nanoporous gold prepared from the Au/Al alloy has large sized channels with few hundreds of nanometers and interconnecting ligaments with pore structure.[38]

### 1.2.4. Ternary alloys

Other than the binary alloys, ternary alloys that contain three metals can also result in nanoporous gold. Ternary alloys like Ag-Au-Pt, Au-Pt-Cu, Al-Au-Pt, Al-Au-Pd, Au-Pd-Ag, were described in the literature.[38-40] Wang and coworkers, for example, have taken Aluminum, Gold, intermetallic precursor, doped with Platinum and Palladium and successive dealloying was done in NaOH/HCl, $HNO_3$ resulting in nanoporous gold with small amounts of platinum and palladium. These materials act as excellent electrocatalysts and show good catalytic activities.[41] Erlebacher and coworkers have used a ternary alloy, Au-Ag-Pt, with platinum containing less than 7%. Adding Platinum to the alloy helps to restructure the gold into thinner ligaments, impedes the diffusion process of gold atoms, and alters the chemical and physical characteristics, structure and morphology.[38] Erlebacher and coworkers also showed by using Al-Au-Pt, Al-Au-Pt (Pd) alloys, a different structure with smaller ligaments and channel sizes can be fabricated compared to other Au-Ag alloys.[38] Stine et al have used definite atomic composition of readily available 10 karat gold alloy, which is a pentanary alloy ( 41.8% Au, 5% Ag, 30–35% Cu, 8–9% Zn, and 15–20% Ni). They dealloyed with nitric acid for 24 hours resulting in nanoporous gold having high surface area of 14.2 $m^2/g$ and

12,400 times surface enlargement; 72 hour nitric acid treatment gave surface area of 8.7 $m^2/g$ and 6900 times surface enlargement.[35]

### 1.2.5. Commerical Au-Ag alloy.

From the literature and history of dealloying it states that there is a bonding between dealloying and depletion gilding.[31,42] According to this view many researchers have focused on commercially available gold and silver alloys of 9-12 karat of gold.[3143] Definite atomic composition of Au:Ag can be readily available (premade) from the art store, jewelry or from other locations, which is 10-12k white gold leaf. White gold leaf can be obtained from art suppliers because they are used for decorative purposes. White gold leaf is prepared by hammering, where it is rolled into 50-100 microns and then hammered to decrease the thickness to around 100 nm.[31] By manufacturing this leaf, the cost of the materials has been decreased by a factor of 10.[31]

### 1.2.6. Dealloying

Dealloying is a corrosion process. It removes the least noble element and forms a open bicontinous microstructure with 3D network of interconnected ligaments with large surface area to volume ratio.[44] This process can be directed electrochemically where the least reactive components gets dissolved when current is applied to the cell.[43,45] Another dealloying procedure involves chemical dealloying and is considered as one of the simplest methods.[34,43,46-48]. Strong acids such as nitric acid or sulfuric acid can be used as an electrolyte medium. The process of dealloying successfully takes place if the alloy composition has a narrow range of~26-36%.[49,50] If atomic percentage of the component A in alloy is greater than 36%, the materials will contain randomly

distributed pores and lack a porous structure. However, at lower than 26%, microscopic cracking was detected.[49,50]

### 1.2.7. Chemical Dealloying

Chemical dealloying is a process where alloy is inserted into strong acids such as nitric acid or sulfuric acid and dissolution of the alloy takes place. There are many different type of alloys used in dealloying (as mentioned in Alloy selection), but majority of the work has been done using Au-Ag alloys. When the binary alloy Au:Ag is dealloyed in nitric acid, the time spent in the nitric acid influences how much silver remains in the framework and the pore/ligament size. The longer the alloy stays in acid, the lower percent of silver and the larger the pore and ligament size. Dealloying at low temperatures can affect the smaller pore sizes, which are ~ 5 nm.[51] Dealloying in diluted acids lead to greater percentage of silver remaining in the nanostructure.[52]

### 1.2.8. Electrochemical Dealloying

Electrochemical dealloying is alternative approach where potential is applied to the electrochemical cell. It can be undertaken in different ways. Pore size and ligament length can be varied by altering the experimental conditions like temperature, applied potential, electrolyte, precursor alloy composition and time. Usually dilute perchloric acid is used. Apart from that, neutral pH silver nitrate solutions and halide containing electrolytes like $AgClO_4/HClO_4$ and $AgNO_3/HNO_3$ can also be used.[45,53-56] When dealloying under elevated temperatures,[56,67,77] it helps to decrease the time[57] the alloy is exposed to acid and the mechanical stability of the film can be

improved.[30,56,58,59,63,67,77] "Four noteworthy features about electrochemical dealloying Au-Ag binary alloys are as follows: (1) the kinetics of the dealloying process can be followed and studied by monitoring the current density resulting from the dissolution of Ag from the alloy surface; (2) the electrolyte solutions chosen are significantly less corrosive than concentrated nitric acid; (3) the nanoporous gold has to be in electrical contact to dealloy; and (4) the pore/ligament structure can be controlled to a certain extent by the magnitude of the applied potential."[30]

### 1.3. Mechanism of pore evolution

The mechanism associated with the formation of pores has been investigated by several research groups. Among them, Erlebacher et al has taken a major role in evaluating the mechanism of pore formation.[60-63] Erlebacher et al has proposed a continuum model, which was fully compatible with both experimental and theoretical simulations involving alloy dissolution. These experiments demonstrated that nanoporosity occurring in metals is due to the intrinsic dynamic pattern, which is involved in the formation process. It is because the more noble atoms are driven to aggregate into two dimensional clusters. This cluster formation is happening because of phase separation at the interface of solid and electrolyte interface. The surface area continuously increases with etching. The porosity started from the dissolution of the least noble atom on the outer most surface of the homogeneous binary systems. The removal of gold atoms forms gold rich clusters at surface surrounded by holes. This process is enhanced at the electrolyte /metal interface position. This results in the

exposure of the remaining Ag, which dissolves and leads to the additional reorganization of the gold atoms at the interface. At the same time, more gold containing clusters turn into mounds. These mounds become undercut, which leads to the formation of new clusters by using holes /pits. This nanoporous gold further develops in this process and silver becomes depleted.[63]

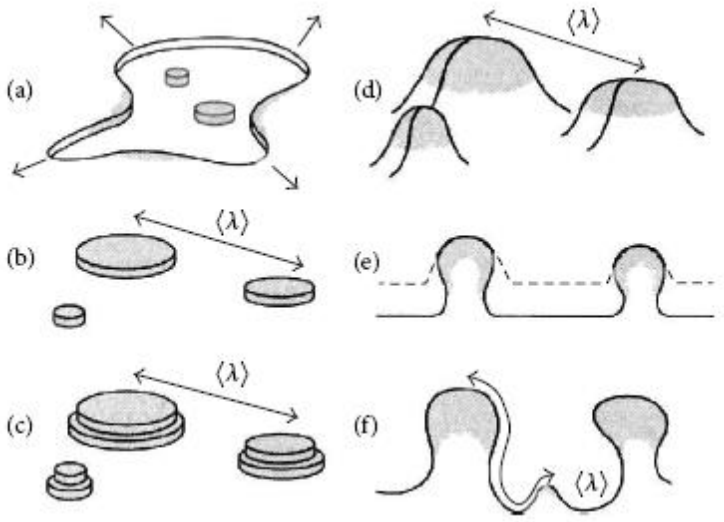


**Figure 1.** Evolution in porosity during the dealloying of Au:Ag alloy. Reproduced by permission of The Electrochemical Society.[63]

## 1.4. Applications

Nanoporous gold has received considerable interest over the years. Presently, many researchers use nanoporous gold in applications such as chemical sensors,[64] biofuel cells[65], fuel cell catalysis,[66] and also in organic synthesis.[67] Nanoporous gold also showed applications in localized surface plasmon resonance (LSPR)[68] and surface-enhanced Raman spectroscopy (SERS).[69] In the development of chemical sensors, nanoporous gold has attained a superlative role. The high conductivity, high surface area, the ability to modify ligament and pore size, and their relatively open structure has allowed them to play an important role in the development of chemical sensors. Nanoporous gold permits a much higher amount of a reagent or analyte to be immobilized on its surface.[43,47,48] This increases the signals compared to a planar gold surfaces. However, at the same time the non-faradaic current, which represents "noise", also scales with the electrode area.

Nanoporous gold is also considered an excellent material for catalytic applications. It has capability to catalyze reactions, but the mechanism of the catalytic activity has not been clearly identified. Some of the important applications include partial oxidation with high selectivity and at low temperature,[70] glucose electrooxidation,[71] critical reaction in fuel cells,[66] reduction of oxygen and hydrogen peroxide,[72] aerobic oxidation of glucose to gluconic acid, oxidation of CO to $CO_2$.[73]

Nanoporous gold with smaller pores and ligaments were more effective compared to the planar gold, towards catalytic oxidation and other catalytic applications.

# References


1. Wisniewski, N.; Moussy, F.; Reichert, W. M. Characterization of implantable biosensor membrane biofouling *Fresenius J. Anal. Chem.* **2000***, 366*, 611-621.

2. Wisniewski, N.; Reichert, M. Methods for reducing biosensor membrane biofouling *Colloids and Surfaces B: Biointerfaces* **2000***, 18*, 197.

3. Rabe, M.; Verdes, D.; Seeger, S. Understanding protein adsorption phenomena at solid surfaces *Adv. Colloid Interface Sci.* **2011***, 162*, 87-106.

4. Sadana, A. Protein adsorption and inactivation on surfaces. Influence of heterogeneities *Chem. Rev.* **1992***, 92*, 1799-1818.

5. Chen, D.; Wang, G.; Li, J. H. Interfacial Bioelectrochemistry: Fabrication, Properties and Applications of Functional Nanostructured Biointerface. *J. Phys. Chem. C* **2007***, 111*, 2351-2367.

6. Nakanishi, K.; Sakiyama, T.; Imamura, K. On the adsorption of proteins on solid surfaces, a common but very complicated phenomenon. *J Biosci Bioeng. 2001;91(3):233-44.* **2001***, 91*, 233-244.

7. Wilson, G. S.; Johnson, M. A. In-Vivo Electrochemistry: What Can We Learn about Living Systems? *Chem. Rev.* **2008***, 108*, 2462-2481.

8. Higson, S. P. J.; Vadgama, P. M. Diamond like carbon coated films for enzyme electrodes; characterization of biocompatibility and substrate diffusion limiting properties *Anal. Chem. Acta* **1995***, 300*, 77-83.

9. Higson, S. P. J.; Vadgama, P. M. Diamond like carbon films for enzyme electrodes; characterisation of novel overlying permselective barriers *Anal. Chem. Acta* **1995***, 300*, 85-90.

10. Higson, S. P. J.; Desai, M. A.; Ghosh, S.; Christie, I.; Vadgama, P. Amperometric enzyme electrode biofouling and passivation in blood: characterisation of working electrode polarisation and inner membrane effects *J. Chem. Soc. Faraday Transactions* **1993***, 89*, 2847.

11. Taniguchi, I.; Yoshimoto, S.; Yoshida, M.; Kobayashi, S.; Miyawaki, T.; Aono, Y.; Sunatsuki, Y.; Taira, H. Simple methods for preparation of a well-defined 4-pyridinethiol modified surface on Au(111) electrodes for cytochrome c electrochemistry *Electrochim. Acta* **2000***, 45*, 2843-2853.

12. Brown, K. R.; Fox, A. P.; Natan, M. J. Morphology-Dependent Electrochemistry of Cytochrome *c* at Au Colloid-Modified $SnO_2$ Electrodes. *J. Am. Chem. Soc.* **1996**, *118*, 1154-1157.

13. Liu; Gooding, J. J. An Interface Comprising Molecular Wires and Poly(ethylene glycol) Spacer Units Self-Assembled on Carbon Electrodes for Studies of Protein Electrochemistry *Langmuir* **2006**, *22*, 7421-7430.

14. Prime, K.; Whitesides, G. Self-assembled organic monolayers: model systems for studying adsorption of proteins at surfaces *Science* **1991**, *252*, 1164-1167.

15. Liu, G.; Böcking, T.; Gooding, J. J. Diazonium salts: Stable monolayers on gold electrodes for sensing applications *J Electroanal Chem* **2007**, *600*, 335-344.

16. Collyer, S.; Davis, F.; Lucke, A.; Stirling, C. J. M.; Higson, S. P. An Investigation into Outer-Surface Biofouling and Electrode Passivation Effects on Gold Electrodes Modified with Calix[4]resorcinarenetetrathiol and a PEG Derivative on Exposure to Whole Human Blood. *J. Electroanalysis* **2004**, *16*, 275-281.

17. Xu, F.; Flanagan, C. E.; Ruiz, A.; Crone, W. C.; Masters, K. S. Polyurethane/Dermatan Sulfate Copolymers as Hemocompatible, Non-Biofouling Materials *Macromolecular Bioscience* **2010**, *11*, 257-266.

18. Patel, J.; Radhakrishnan, L.; Zhao, B.; Uppalapati, B.; Daniels, R. C.; Ward, K. R.; Collinson, M. M. Electrochemical Properties of Nanostructured Porous Gold Electrodes in Biofouling Solutions *Anal. Chem.* **2013**, *85*, 11610-11618.

19. Jia, F.; Yu, C.; Deng, K.; Zhang, L. Nanoporous Metal (Cu, Ag, Au) Films with High Surface Area: General Fabrication and Preliminary Electrochemical Performance. *J. Phys. Chem.* **2007**, *111*, 8424-8431.

20. Wittstock, A.; Biener, J.; Baumer, M. Nanoporous gold: a new material for catalytic and sensor applications *Phys. Chem. Chem. Phys.* **2010**, *12*, 12919-12930.

21. Choi, M.; Ryoo, R. Ordered nanoporous polymer-carbon composites *Nat. Mater.* **2003**, *2*, 473-476.

22. Scanlon, M. D.; Salaj-Kosla, U.; Belochapkine, S.; MacAodha, D.; Leech, D.; Ding, Y.; Magner, E. Characterization of Nanoporous Gold Electrodes for Bioelectrochemical Applications *Langmuir* **2012**, *28*, 2251-2261.

23. Stewart, M. P.; Buriak, J. M. Chemical and Biological Applications of Porous Silicon Technology. *Adv. Mater* **2000**, *12*, 859-869.

24. Sing, K. S. W. Reporting physisorption data for gas/solid systems with special reference to the determination of surface area and porosity (Recommendations 1984) *Pure and Applied Chemistry* **1985;** *57*, 603-619.

25. Bartlett, P. N.; Baumberg, J. J.; Birkin, P. R.; Ghanem, M. A.; Netti, M. C. Highly Ordered Macroporous Gold and Platinum Films Formed by Electrochemical Deposition through Templates Assembled from Submicron Diameter Monodisperse Polystyrene Spheres *Chemistry of Materials* **2002**, *14*, 2199-2208.

26. Zhao, B.; Collinson, M. M. Hierarchical porous gold electrodes: Preparation, characterization, and electrochemical behavior *J Electroanal Chem* **2012***, 684*, 53-59.

27. Kim, M.; Jeong, G. H.; Lee, K. Y.; Kwon, K.; Han, S. W. Fabrication of nanoporous superstructures through hierarchical self-assembly of nanoparticles *Journal of Materials Chemistry* **2008***, 18*, 2208.

28. Murata, K.; Kajiya, K.; Nukaga, M.; Suga, Y.; Watanabe,T.; Nakamura, N.; Ohno, H. A Simple Fabrication Method for Three-Dimensional Gold Nanoparticle Electrodes and Their Application to the Study of the Direct Electrochemistry of Cytochrome C *Electroanalysis* **2009,** 22, 185.

29. Schröper, F.; Brüggemann, D.; Mourzina, Y.; Wolfrum, B.; Offenhäusser, A.; Mayer, D. Analyzing the electroactive surface of gold nanopillars by electrochemical methods for electrode miniaturization *Electrochim. Acta* **2008***, 53*, 6265-6272.

30. Collinson, M. M. Nanoporous Gold Electrodes and Their Applications in Analytical Chemistry. *ISRN Analytical Chemistry* **2013***, 2013*, 21.

31. Ding, Y.; Kim, Y. J.; Erlebacher, J. Nanoporous Gold Leaf: "Ancient Technology"/Advanced Material. **2004***, 16*, 1897-1900.

32. Huang, J., F; Sun, I., W. Fabrication and Surface Functionalization of Nanoporous Gold by Electrochemical Alloying/Dealloying of Au–Zn in an Ionic Liquid, and the Self-Assembly of L-Cysteine Monolayers. *Advanced functional materials* **2005***, 15*, 989-994.

33. Zhang, Z.; Wang, Y.; Qi, Z.; Somsen, C.; Wang, X.; Zhao, C. Fabrication and characterization of nanoporous gold composites through chemical dealloying of two phase Al–Au alloys *Journal of Materials Chemistry* **2009***, 19*, 6042.

34. Rouya, E.; Reed, M. L.; Kelly, R. G.; Bart-Smith, H.; Begley, M.; Zangari, G. Synthesis of Nanoporous Gold Structures via Dealloying of Electroplated Au-Ni Alloy Films *ECS Transactions;* 2007; Vol. 6, pp 41-50.

35. Shulga, O. V.; Jefferson, K.; Khan, A. R.; D'Souza, V. T.; Liu, J.; Demchenko, A. V.; Stine, K. J. Preparation and Characterization of Porous Gold and its Application as a Platform for Immobilization of Acetylcholine Esterase *Chem. Mater.* **2007***, 19*, 3902-3911.

36. Zhang, Z.; Wang, Y.; Qi, Z.; Lin, J.; Bian, X. Nanoporous Gold Ribbons with Bimodal Channel Size Distributions by Chemical Dealloying of Al-Au Alloys *The Journal of Physical Chemistry C* **2009***, 113*, 1308-1314.

37. Zhang, Z.; Wang, Y.; Qi, Z.; Lin, J.; Bian, X. Nanoporous Gold Ribbons with Bimodal Channel Size Distributions by Chemical Dealloying of Al-Au Alloys *The Journal of Physical Chemistry C* **2009***, 113*, 1308-1314.

38. Snyder, J.; Asanithi, P.; Dalton, A. B.; Erlebacher, J. Stabilized Nanoporous Metals by Dealloying Ternary Alloy Precursors *Adv Mater* **2008***, 20*, 4883-4886.

39. Wang, X.; Wang, W.; Qi, Z.; Zhao, C.; Ji, H.; Zhang, Z. High catalytic activity of ultrafine nanoporous palladium for electro-oxidation of methanol, ethanol, and formic acid *Electrochemistry Communications* **2009**, *11*, 1896-1899.

40. Xu, J.; Zhang, C.; Wang, X.; Ji, H.; Zhao, C.; Wang, Y.; Zhang, Z. Fabrication of bi-modal nanoporous bimetallic Pt–Au alloy with excellent electrocatalytic performance towards formic acid oxidation *Green Chem.* **2011**, *13*, 1914.

41. Wang, X.; Frenzel, J.; Wang, W.; Ji, H.; Qi, Z.; Zhang, Z.; Eggeler, G. Length-Scale Modulated and Electrocatalytic Activity Enhanced Nanoporous Gold by Doping *The Journal of Physical Chemistry C* **2011**, *115*, 4456-4465.

42. Zhang, Z.; Wang, Y.; Qi, Z.; Zhang, W.; Qin, J.; Frenzel, J. Generalized Fabrication of Nanoporous Metals (Au, Pd, Pt, Ag, and Cu) through Chemical Dealloying *The Journal of Physical Chemistry C* **2009**, *113*, 12629-12636.

43. Seker, E.; Reed, M. L.; Begley, M. R. Nanoporous Gold: Fabrication, Characterization, and Applications *Materials* **2009**, *2*, 2188-2215.

44. Erlebacher, J. An Atomistic Description of Dealloying *J. Electrochem. Soc.* **2004**, *151*, C614.

45. Dursun, A.; Pugh, D. V.; Corcoran, S. G. A Steady-State Method for Determining the Dealloying Critical Potential *Electrochemical and Solid-State Letters* **2003**, *6*, B32.

46. Li, X.; Yang, X.; Zhang, S. Electrochemical enzyme immunoassay using model labels *TrAC Trends in Analytical Chemistry* **2008**, *27*, 543-553.

47. Luppa, P. B.; Sokoll, L. J.; Chan, D. W. Immunosensors—principles and applications to clinical chemistry *Clinica Chimica Acta* **2001**, *314*, 1-26.

48. Ronkainen, N. J.; Halsall, H. B.; Heineman, W. R. Electrochemical biosensors *Chem. Soc. Rev.* **2010**, *39*, 1747-1763.

49. Lu, X.; Balk, T. J.; Spolenak, R.; Arzt, E. Dealloying of Au–Ag thin films with a composition gradient: Influence on morphology of nanoporous Au *Thin Solid Films* **2007**, *515*, 7122-7126.

50. Lu, X.; Bischoff, E.; Spolenak, R.; Balk, T. J. Investigation of dealloying in Au–Ag thin films by quantitative electron probe microanalysis *Scr. Mater.* **2007**, *56*, 557-560.

51. Qian, L. H.; Chen, M. W. Ultrafine nanoporous gold by low-temperature dealloying and kinetics of nanopore formation *Appl. Phys. Lett.* **2007**, *91*, 083105.

52. Dixon, M. C.; Daniel, T. A.; Hieda, M.; Smilgies, D. M.; Chan, M. H. W.; Allara, D. L. Preparation, Structure, and Optical Properties of Nanoporous Gold Thin Films *Langmuir* **2007**, *23*, 2414-2422.

53. Sieradzki, K.; Dimitrov, N.; Movrin, D.; McCall, C.; Vasiljevic, N.; Erlebacher, J. The Dealloying Critical Potential *J. Electrochem. Soc.* **2002**, *149*, B370.

54. Wagner, K. Dealloying below the Critical Potential *J. Electrochem. Soc.* **1997**, *144*, 3545.

55. McCall, C.; Dimitrov, N.; Sieradzki, K. Underpotential Deposition on Alloys *J. Electrochem. Soc.* **2001***, 148*, E290.

56. Snyder, J.; Livi, K.; Erlebacher, J. Dealloying Silver/Gold Alloys in Neutral Silver Nitrate Solution: Porosity Evolution, Surface Composition, and Surface Oxides *J. Electrochem. Soc.* **2008***, 155*, C464.

57. Li, R.; Sieradzki, K. Ductile-brittle transition in random porous Au *Phys. Rev. Lett.* **1992***, 68*, 1168-1171.

58. Senior, N. A.; Newman, R. C. Synthesis of tough nanoporous metals by controlled electrolytic dealloying *Nanotechnology* **2006,** *17*, 2311-2316.

59. Kim, M.; Ha, W.; Anh, J.; Kim, H.; Park, S.; Lee, D. Fabrication of nanoporous gold thin films on silicon substrate by multilayer deposition of Au and Ag *J. Alloys Compounds* **2009***, 484*, 28-32.

60. Erlebacher, J.; Aziz, M. J.; Karma, A.; Dimitrov, N.; Sieradzki, K. Evolution of nanoporosity in dealloying *Nature* **2001***, 410*, 450-453.

61. Erlebacher, J.; Sieradzki, K. Pattern formation during dealloying *Scr. Mater.* **2003***, 49*, 991-996.

62. Parida, S.; Kramer, D.; Volkert, C.; Rösner, H.; Erlebacher, J.; Weissmüller, J. Volume Change during the Formation of Nanoporous Gold by Dealloying *Phys. Rev. Lett.* **2006***, 97*.

63. Erlebacher, J. An Atomistic Description of Dealloying *J. Electrochem. Soc.* **2004***, 151*, C614.

64. van Noort, D.; Rani, R.; Mandenius, C. Improving the Sensitivity of a Quartz Crystal Microbalance for Biosensing by Using Porous Gold *Microchimica Acta* **2001***, 136*, 49-53.

65. Qiu, H.; Xu, C.; Huang, X.; Ding, Y.; Qu, Y.; Gao, P. Immobilization of Laccase on Nanoporous Gold: Comparative Studies on the Immobilization Strategies and the Particle Size Effects *The Journal of Physical Chemistry C* **2009***, 113*, 2521-2525.

66. Wittstock, A.; Zielasek, V.; Biener, J.; Friend, C. M.; Baumer, M. Nanoporous Gold Catalysts for Selective Gas-Phase Oxidative Coupling of Methanol at Low Temperature *Science* **2010***, 327*, 319-322.

67. Pornsuriyasak, P.; Ranade, S. C.; Li, A.; Parlato, M. C.; Sims, C. R.; Shulga, O. V.; Stine, K. J.; Demchenko, A. V. STICS: surface-tethered iterative carbohydrate synthesis *Chemical Communications* **2009**, 1834.

68. Willets, K. A.; Duyne, V. Localized Surface Plasmon Resonance Spectroscopy and Sensing - Annual Review of Physical Chemistry, 58(1):267. *Annual Review of Physical Chemistry.* **2007***, 58*, 267-297.

69. Qian, L., H.; Yan, X. Q.; Fujita, T.; Inoue, A.; Chen, M. W. Surface enhanced Raman scattering of nanoporous gold: Smaller pore sizes stronger enhancements. *Qian LH, Yan XQ, Fujita T, Inoue A, Chen MW.* **2007***, 90*, 153120.

70. Wittstock, A.; Zielasek, V.; Biener, J.; Friend, C. M.; Baumer, M. Nanoporous Gold Catalysts for Selective Gas-Phase Oxidative Coupling of Methanol at Low Temperature *Science* **2010; 2010***, 327*, 319-322.

71. Seo, B.; Kim, J. Electrooxidation of Glucose at Nanoporous Gold Surfaces: Structure Dependent Electrocatalysis and Its Application to Amperometric Detection *Electroanalysis* **2010***, 22*, 939-945.

72. Zeis, R.; Lei, T.; Sieradzki, K.; Snyder, J.; Erlebacher, J. Catalytic reduction of oxygen and hydrogen peroxide by nanoporous gold *Journal of Catalysis* **2008***, 253*, 132-138.

73. Yin, H.; Zhou, C.; Xu, C.; Liu, P.; Xu, X.; Ding, Y. Aerobic Oxidation of d-Glucose on Support-Free Nanoporous Gold - The Journal of Physical Chemistry C (ACS Publications) *The Journal of Physical Chemistry C* **2008***, 112*, 9673.

# Chapter 2: Fabrication and Characterization

## 2.1. Introduction

Nanoporous gold materials can be fabricated by different methods, such as dealloying, thermal deposition of gold oxide, sublimation of iodine from gold iodide pressed powders, and dissolution of gold chloride in a dextran solution followed by heating to higher temperatures.[1-4] Among different fabrication methods, dealloying is the simplest method. Nanoporous gold possesses unique chemical and physical properties such as large specific surface area, high surface-to-volume ratio, strength, and ductility. Nanoporous gold exhibits wide range of applications in various fields, supercapacitors,[5] catalysis,[6-8] batteries,[9] and sensors.[10-12]

In our work, nanoporous gold is formed by selective removal of one or more less noble elements that are present along with gold. We have used an Au/Ag alloy that we selectively etch in nitric acid for a given period of time followed by rinsing with water. Dealloying proceeds as the surface tension of liquid evenly spreads over the surface of the leaf. Gold restructures itself through surface diffusion leading to three dimensional networks with interconnected ligaments.[13]

The dealloying time plays a major role in determining the pore size, ligament size and surface area. During the time the gold-silver alloy is in nitric acid, gold atoms

restructure themselves due to surface diffusion and the silver is removed. The longer the time in nitric acid, the more silver is removed and the structure of the nanoporous gold changes. The concentration of the nitric acid also influences the formation of nanoporous gold; higher concentrations are needed for dealloying to take place. We have also found that the manner at which the white gold leaf alloy sits in the nitric acid effects pore morphology. Floating the leaf on surface of nitric acid vs pushing it underneath gives different results. We have inserted the leaf into nitric acid so that pores are completed evolved from top and bottom of the leaf. Careful control over the pore size is required as described below. During fabrication of nanoporous gold films, the color of the gold leaf changes from white to either light or dark brown. As described below, a dark brown leaf gives rise to nanoporous gold with small pores and high surface area whereas light brown leaf has larger pores and a smaller surface area. This observation led to a further study of the fabrication process on nanoporous gold.

In this chapter, the fabrication of nanoporous gold electrodes at different dealloying times is described, which gives rise to differences in the surface area, structure, and morphology of nanoporous gold. Characterization of the nanoporous gold morphology, composition, and structure was performed with X-ray photoelectron spectroscopy (XPS) scanning electron microscopy (SEM), and Energy-dispersive X-ray spectroscopy (EDX). Surface areas of a variety of different nanoporous gold films were measured electrochemically.

### 2.1.1 Experimental: Materials

Manetti 12 Karat gold leaf (50 wt% Au:50 wt% Ag) was purchased from Fine Art Store. Gold mirror electrodes with a Ti adhesion layer were purchased from EMF Corporation. Nitric acid (69.3% w/v) was purchased from Fisher Scientific. Water was purified using a Millipore water purification system.

### 2.1.2 Preparation of nanoporous gold electrodes:

Nanoporous gold electrodes were fabricated via dealloying 12 K gold leaf in concentrated nitric acid for a specific time as described by Erlebacher.[14,15] In this work, an inexpensive source of thin Au-Ag alloy i.e. "white-gold" leaves sold at art stores for decorative purposes was used. These alloy leaves, which come in a booklet of 25, are 10 cm X 10 cm in size. The elemental composition of the alloy leaf is annotated by its karat value (e.g., 12-kt white gold has equal weights of gold and silver). The gold coated slide obtained from EMF Corporation was carefully cut into 2.5 cm length X 0.5 cm width pieces. Microscopic glass slides were cut into 0.5 x 0.5 cm. These slides (both glass and gold) were placed in ethanol (200% proof) and sonicated for 10 min followed by sonication in an ethanol-water mixture (10:90) for about 10 min. After sonication, the slides were introduced into pure deionized water and again sonicated for 10 min. After completion of these sonication cycles, the planar gold electrodes and/or glass slides were removed and dried in a stream of nitrogen gas. This process cleans the surfaces so they will be ready to use for the preparation of nanoporous Au. The glass slides after sonication were placed in a clean petri dish. The Ag-Au alloy leaves were

then cut into 0.3 x 0.3 cm and placed in a small glass petri dish containing deionized water.

A schematic representation of the fabrication of nanoporous gold is shown in Figure 2.1. A pair of leaves (single batch) was placed in a petri dish of deionized water for 10 minutes. For the next batch, the deionized water was removed and replaced with new water. Figure 2.1 shows that glass slides are used to remove the gold leaves from water and to place them in concentrated nitric acid. Each glass slide holds a single gold leaf. Two gold leaves were inserted in a petri dish containing nitric acid. The nitric acid used for dealloying was safely disposed after the process for every batch. After carefully inserting the gold leaf into nitric acid, the leaf floats on nitric acid and with the help of tweezers, the leaf is inserted to the bottom of the dish within 30 seconds. As depicted in Figure 2.1, the gold leaves settle to the bottom of the petri dish. Gold leaves were dealloyed in concentrated (69.3% w/v) nitric acid at different time periods 5, 7, 10, 12.5, and 20 min at 298 K. Gold leaf dealloying time was varied to examine its effect on the surface area and pore size variability. After the specific time period, the gold leaves (pair) were removed by glass slides from the nitric acid and placed in a petri dish containing deionized water for 10 minutes. For every new batch (pair of leaves) fresh deionized water was used. The floating free-standing nanoporous gold leaves were attached to gold coated slide and then allowed to dry naturally at room temperature on the bench top. After ensuring complete dryness, these nanoporous gold electrodes were placed under a UV lamp (254 nm, 20 W) at a distance 5 cm for 24 hours. Planar gold electrodes were used as comparisons to nanoporous gold electrodes.

Planar gold electrodes were plasma cleaned at 10 W for 2 minutes and was placed under the UV light for 24 hours. Plasma cleaning and UV cleaning were considered to be the best methods to clean the electrodes to obtain consistent results. After 24 hours under UV radiation, the nanoporous Au and planar gold electrodes were removed and placed outside in room temperature for the further electrochemical and surface area measurements. An $1/8^{th}$ inch diameter hole was punched into a piece of Hyde tape and the nanoporous gold electrode was covered with that tape and wrapped with parafilm. so that only $1/8^{th}$ inch area was exposed to the electrolyte solution.

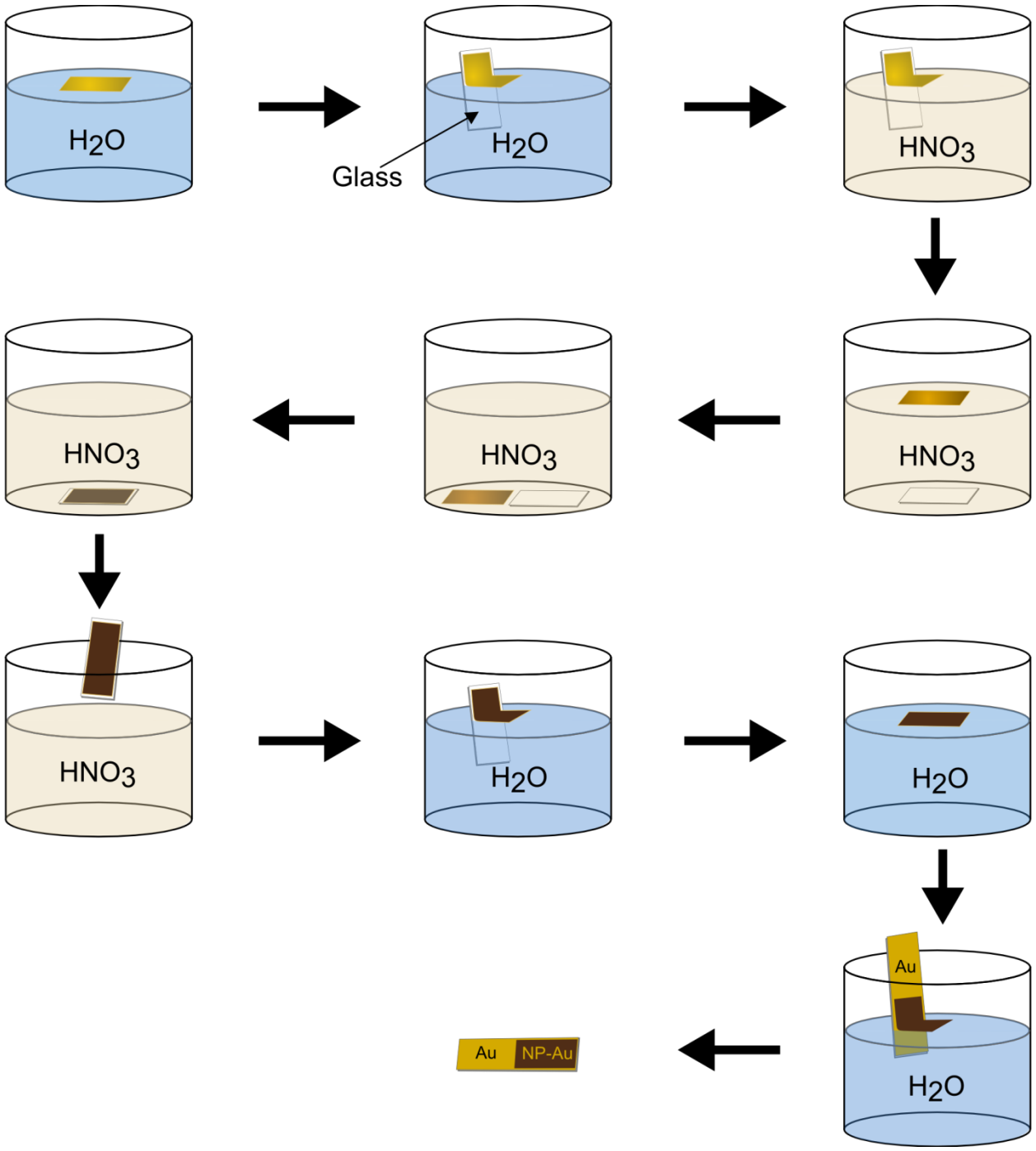


**Figure 2.1** Schematic representation of preparation of nanoporous gold

### 2.1.3 Description of Color

12 karat white gold leaf was used in the preparation of nanoporous gold. The white gold leafs are silver in color. Through the process of dealloying in nitric acid, the gold leaf gradually changes color to dark brown. The dealloying time of the leaf in nitric acid influences the color of the film; color appears due to small size of pores compared to wavelength of light. The color of the film slowly changes from silver to brown after a minute it is immersed in nitric acid. After a few minutes of dealloying the film in nitric acid, the leaf gradually changes to either dark brown or light brown depending upon the dealloying conditions. Two types of color leaves, dark brown and light brown, appeared with same dealloying time. If the film is directly immersed to bottom of the petri dish containing nitric acid in the first 20-30 seconds, it would be dark brown in color or else if delayed more than 30 seconds or if not immersed into bottom of petri dish (allowed to float on nitric acid) it remains light brown in color. If the dealloying time was 10 minutes or greater, the pore size and residual silver can be clearly distinguished by SEM and XPS evaluation.

## 2.2 Results: Overview

The structure, morphology, and chemical composition of the nanoporous gold electrodes were studied using different methods that included scanning electron microscopy (SEM), Energy dispersive X-ray spectroscopy (EDX) and X-ray photoelectron spectroscopy (XPS). The amount of silver present after dealloying of the 12 karat gold was evaluated using both XPS and SEM-EDX methods. These techniques are different

from each other in that XPS gives the information about composition of the surface (top few nanometers), whereas EDX gives information about bulk composition of nanoporous gold. The Au pore and ligament sizes were measured using ImageJ software. Electrochemical measurements were performed using a multichannel potentiostat. Cyclic voltammetry was used to measure the surface area of nanoporous gold.[16,17] Comparisons were made to planar gold.

### 2.2.1 Scanning Electron Microscopy (SEM)

Scanning electron microscopy is a type of electron microscopy that uses a beam of electrons focused on a sample to produce a high resolution image of that sample.[1819,20] Atoms in the sample interact with electrons, which eventually leads to signals that contain information about the surface of the sample, topography as well as composition. A raster scan pattern is generally used by the electron beam. Essential components of all SEMs include the following: Electron Source ("Gun"), which produces multiple, bunches of electrons at a given time. Electron Lenses, sample stage, and detectors for all signals of interest and display / data output devices are the most required components for a routine SEM.[20-22]

A common mode in scanning electron microscopy involves focusing a high energy electron beam on a sample and collecting secondary electrons emitted by the sample.[19,20] The number of secondary electron is dependent on the angle between the surface and the beam. Generally on a flat surface, secondary electrons are mostly contained by the sample, but on a tilted sample, one part of the sample is partially exposed and more electrons are emitted. SEM images of high quality can be obtained.

The sample should be electrically conductive to prevent surface charging. By scanning the sample and detecting the secondary electrons, an image surface can be created. Secondary electrons, back-scattered electrons, characteristic X-rays are the types of electrons produced by a scanning electron microscope. By using SEM, the resolution that can be reached is stated to be on the 1 nanometer scale.[18,21]

In my work, a Hitachi SU-70 field emission scanning electron microscope was used for SEM studies. Typically, samples were cut into 5 mm to 7 mm squares or rectangles. Samples were linked to carbon tape and the corners of the sample were attached to carbon tape to minimize the charging effects. Beam voltages were set as low as 2, 3 and 5 KV and 3-5 mm working distances were maintained. Dealloying times were varied to study the structure and morphology of nanoporous gold structures. The process of dealloying starts as soon as the samples are immersed in nitric acid. From the literature it states; "after immersing the film in nitric acid for one minute, pores appeared to be visible because of removal of silver from the alloy".[23]

To study the pore size variability, films were dealloyed either at 7.5, 10, 12.5, 15, 20 min. Figure 2.2 shows SEM images of the surface of nanoporous gold prepared under different dealloying times. The pore and ligament size appeared to increase as the dealloying time was increased. By using the same alloy composition (12 karat gold) and varying the dealloying times in nitric acid, a wide range of pore and ligament sizes were formed.

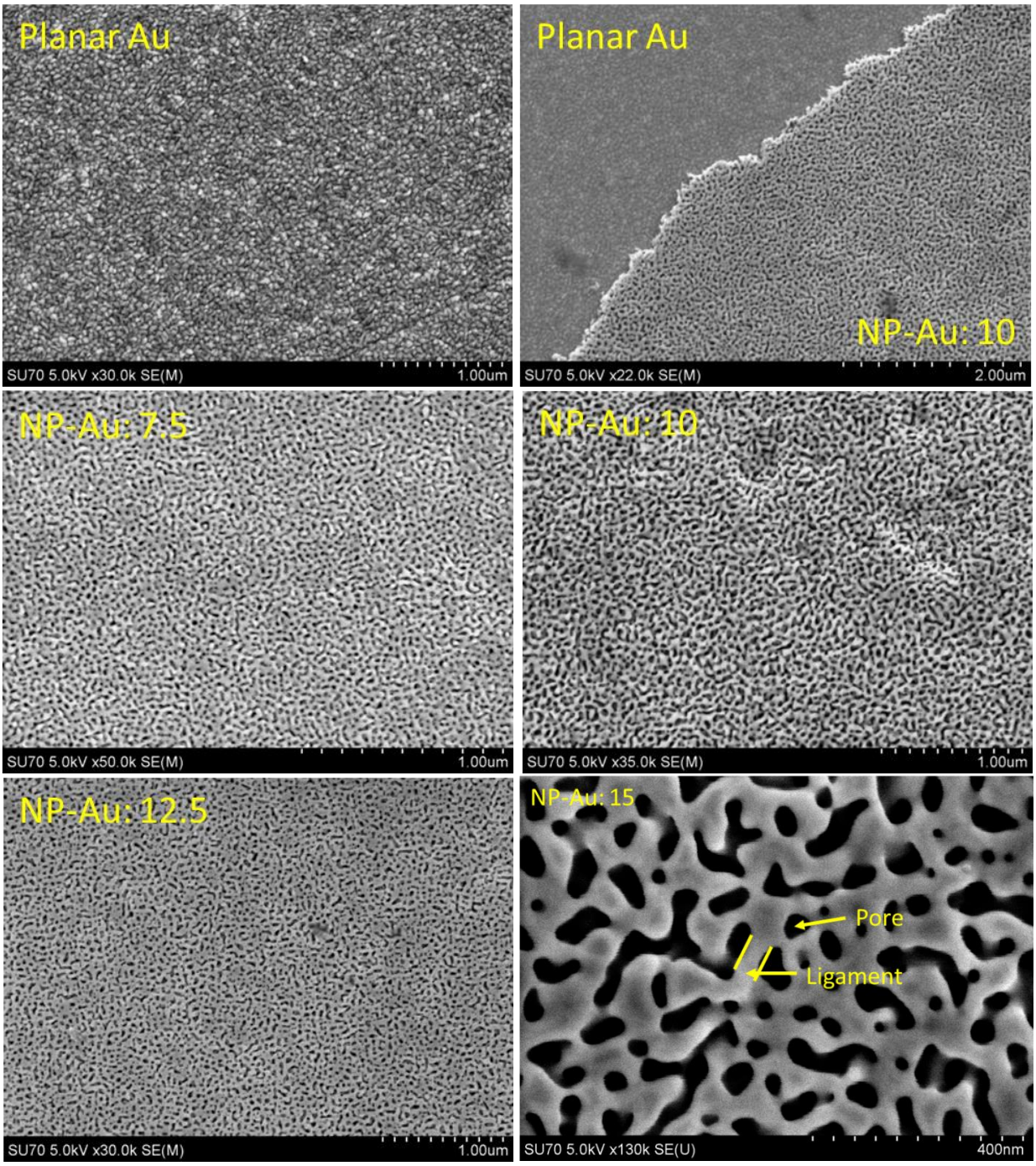


**Figure 2.2** SEM images of the surface of planar Au and nanoporous gold dealloyed for 7.5, 10, 12.5, and 15 in nitric acid.

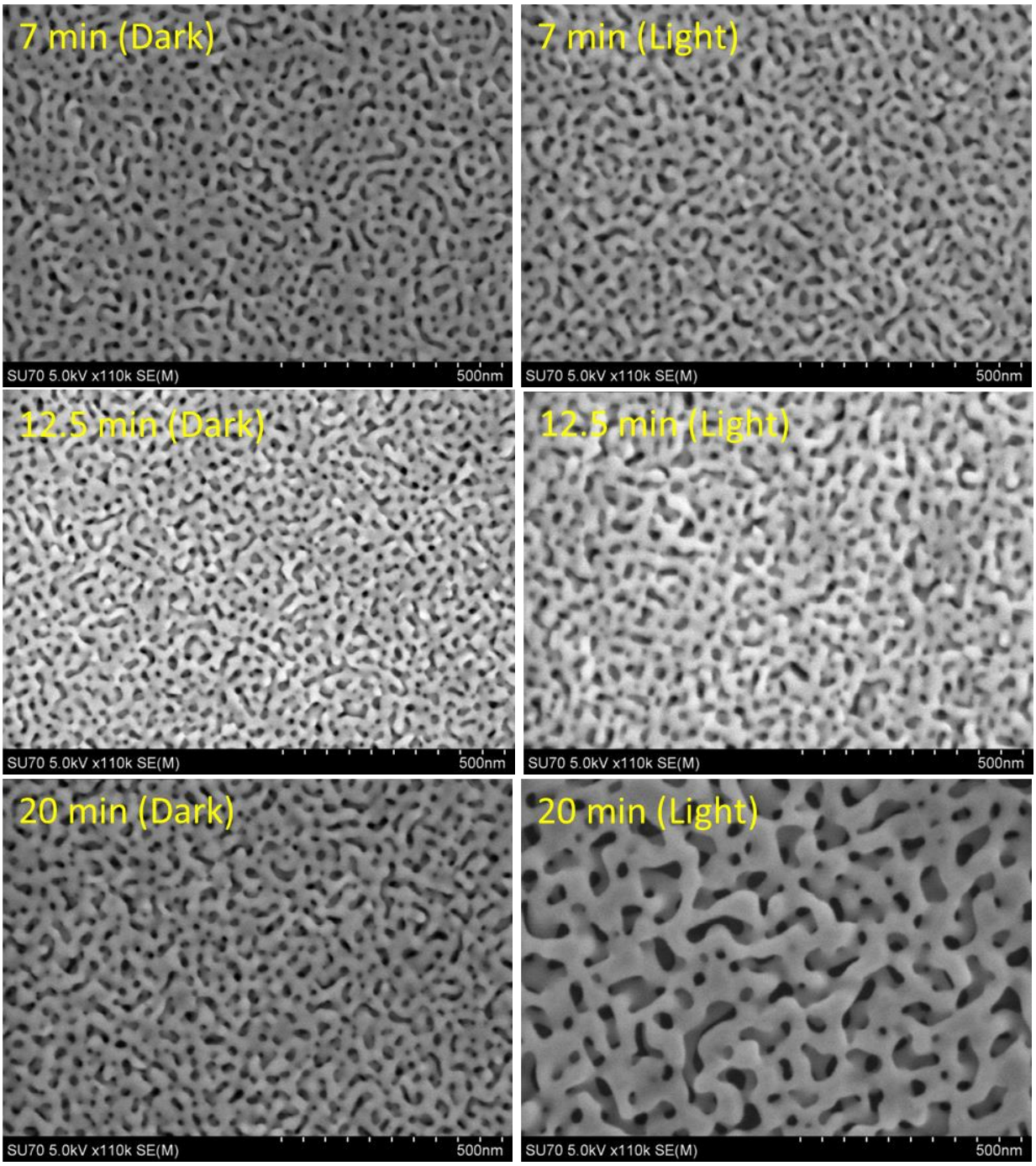


**Figure 2.3** SEMS of Np-Au: 7.5, NP-Au: 12.5, NP-Au: 20 min dealloyed in nitric acid with different dealloying conditions.

Figure 2.3 shows SEM images of 'dark' and 'light' nanoporous gold that that were dealloyed in nitric acid for 7, 12.5 and 20 min. After the leaf is placed in nitric acid. First the leaf floats then slowly the leaf is pushed using tweezers to the bottom of the petri dish (this happens in 30 seconds), if the leaf pushing into the bottom of petri dish is delayed then it showed a big difference in the color (lighter brown), whereas immediate pushing of the film into nitric acid with in 30 seconds made it appear darker brown in color. As can be seen, a difference in the pore and ligament size was observed. Table 2.1 shows pore and ligament size of nanoporous gold at different dealloying times for the two different color leaves. 'Light' leaf showed slightly larger pore and ligament sizes compared to 'dark' leaf. When the dealloying times were increased to 12.5 min or 20 min from 7.5 min, the pores extended deeper into the film and fashioned to be in good interconnected pore framework.

**Table 2.1** Pore and ligament size of nanoporous gold.

| Electrode | Pore size (nm) | Ligament size (nm) |
|---|---|---|
| NPG-7.5 min dark | 5 - 35 | 20 – 50 |
| NPG-7.5 min light | 5 - 50 | 25 – 60 |
| NPG-12.5 min dark | 10 - 40 | 10 – 40 |
| NPG-12.5 min light | 15 - 50 | 15 – 50 |
| NPG-20 min dark | 20 - 70 | 30 – 70 |
| NPG-20 min light | 30 - 100 | 30 – 110 |

### 2.2.2 Energy-dispersive X-ray spectroscopy (EDX)

Energy-dispersive X-ray spectroscopy (EDX) is an analytical technique used for the elemental analysis or chemical characterization of an organic, inorganic or biological sample.[20] In EDX, the sample is excited by electron beam and the characteristic emission of high energy bands are measured. EDX is considered to be an important tool in characterizing the elemental composition of a material.[24]

The Hitachi SU-70 field emission scanning electron microscope was used for SEM-EDX studies. Dealloyed samples of 10 and 12.5 min nanoporous gold were taken for SEM-EDX studies. Different spots were studied on the same sample. One of the reasons EDX studies were done was to know the bulk concentration of nanoporous gold and to verify the consistency of silver and gold atomic % in the various samples. Figure 2.4 shows EDX of NP Au gold dealloyed for 12.5 min. Table 2.2 shows the atomic composition of silver at the various dealloying times. From EDX studies, it can be clearly seen that the silver was removed from the alloy during dealloying process and only ~ 1% of silver is present after dealloying 12.5 min.

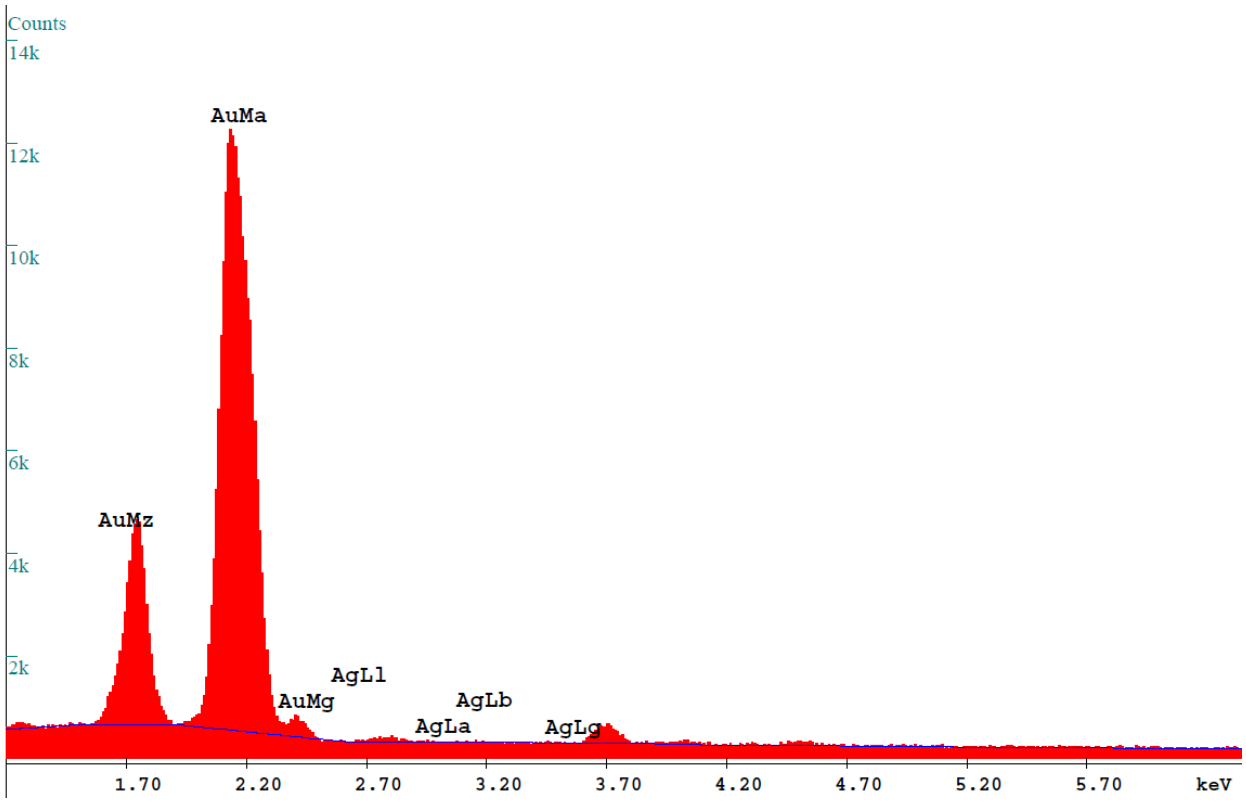


**Figure 2.4** EDX results of nanoporous gold dealloyed for 12.5 min .

**Table 2.2** EDX results showing atomic Ag% of nanoporous gold at 10, 12.5, and 15 min dealloying times.

| Sample | Atomic Ag % |
|---|---|
| NP Au - 10 min | $4 \pm 0.7\%$ |
| NP Au - 12.5 min (Dark) | $1 \pm 0.4\%$ |
| NP Au - 12.5 min (Light) | $1 \pm 0.4\%$ |
| NP Au – 15 min | $0.9 \pm 0.06\%$ |

### 2.2.3 X-ray Photoelectron Spectroscopy (XPS)

X-ray photoelectron spectroscopy (XPS)[25] is sensitive quantitative technique that measures the elemental composition of a sample at the range of parts per thousands on the top few (7-10) nm of a surface. It is also known as Electron spectroscopy for Chemical Analysis (ESCA), and is a widely used a surface analysis technique.[25,26] XPS can be used to determine the empirical formula of a compound, chemical state and electron state of elements.[25,26] The sample is irradiated with mono-energetic X-rays. These x-rays cause the photoelectrons to be emitted from the sample surface. An electron analyzer analyses the binding energy and intensity of the photoelectrons, which are knocked from the outer shell orbital's of atoms in a given sample. Every element produces a characteristic set of XPS peaks.[26,27] These peaks correspond to the binding energy values that directly identify each element that exists on the surface of a given sample. Figure 2.5 shows a schematic representation of the XPS process. These characteristic spectral peaks correspond to the respective electronic configuration of the electrons within the atoms, e.g., 1s, 2s, 2p, 3s, etc. The number of detected electrons in each of the characteristic peaks is directly related to the amount of element in the XPS sample. To obtain the atomic percentage values, each raw XPS signal must be corrected by dividing its signal intensity by a "relative sensitivity factor" (RSF)[25]. Based on the binding energy and intensity of a photoelectron peak, the elemental identity, the chemical state of an atom and quantity of the element present in the sample can be determined.

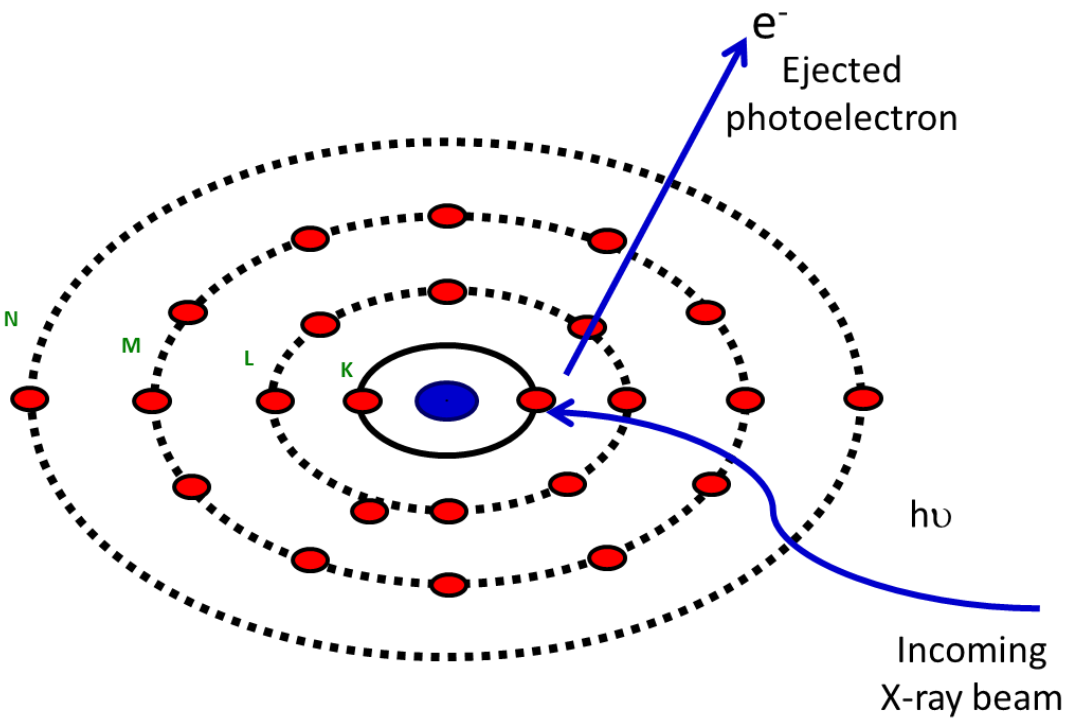


**Figure 2.5:** Schematic representation of XPS process

XPS instruments include a beam of monochromatic aluminum Kα X-rays or magnesium Kα X-rays. Energy of an X-ray with particular wavelength is known (for aluminum Kα X-rays, E photon = 1486.7 eV), the electron binding energy of each of the emitted electrons can be determined by using an equation that has been based on Ernest Rutherford.

$$E\ (\text{binding}) = E\ (\text{photon}) - E\ (\text{kinetic}) + \emptyset$$

where E(binding energy, BE) of the electron, E photon is the energy of the X-ray photons being used, E kinetic is the kinetic energy of the electron as measured by the instrument and phi is the work function of the spectrometer.

XPS analysis was performed with a ThermoFisher ESCAlab 250 imaging X-ray photoelectron spectrometer (Al K$\alpha$ (146.68 eV), 500 µm spot size, 50 eV pass energy, 0.1 eV step size). Typically samples were 5 mm to 7 mm squares or rectangles. CASA software (Version 2.3.15) was used to obtain peak area. Background correction was used by integration of all the peaks. Shirley background type gives a S-shaped background type. Silver and gold peaks binding energies were referenced while adjusting to carbon 1s binding energy 284.5 eV. Atomic sensitivity factors for Ag 3d and Au 4f were 5.2 and 4.95, respectively. %Ag and %Au were calculated using the formula

$$\%\text{Ag} = \frac{\frac{\%\text{Ag}}{5.2}}{\frac{\%\text{Au}}{4.95} + \frac{\%\text{Ag}}{5.2}}$$

where Au and Ag were XPS peak areas taken after background correction using CASA

software. Multiple spots were taken from the same sample and averaged to determine the exact atomic % of silver in each of the samples. Table 2.3 shows the %Ag and %Au of dealloyed samples 7.5, 10, 12.5, and 20 min (NP-Au:7.5, Np-Au:10, NP-Au:12.5, NP-Au:20). From the Table 2.3, it can be seen that Ag is removed from the alloy during the dealloying process and~4-15% Ag remains depending on the time in nitric acid. Further studies were also investigated based on color of the nanoporous gold. Figure 2.6 shows overlaying images of Ag light and dark & Au light and dark of nanoporous gold at 7.5, 10, 12.5, 20 min dealloying times. As the dealloying time increased, a smaller percentage of silver remains on the top surface of nanoporous gold. These nanoporous gold leaves are lighter brown in color compared to darker brown color leaves, which show a higher amount of silver. Table 2.3 clearly shows the majority of the silver present in nanoporous gold are from leaves that were etched at shorter dealloying times.

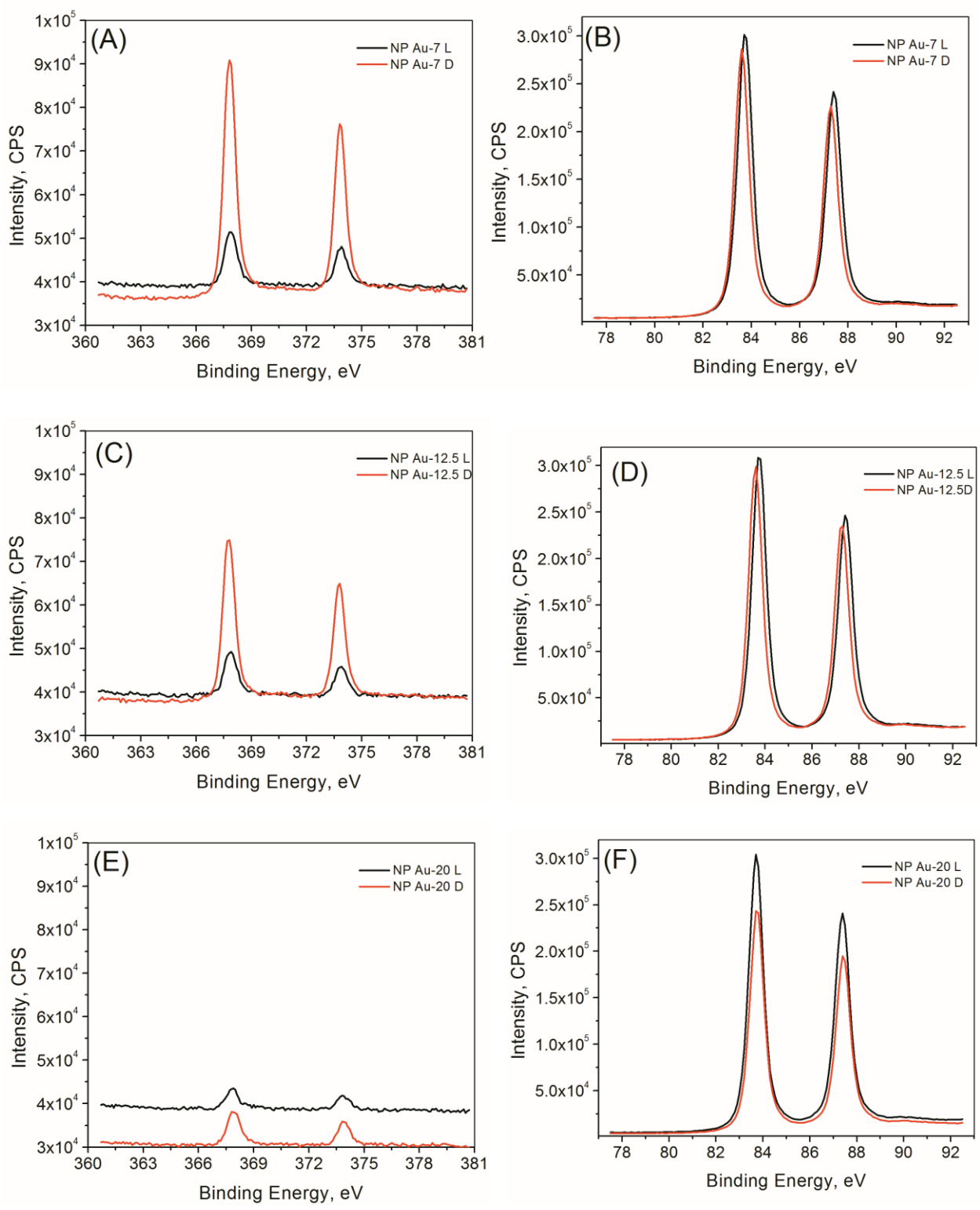


**Figure 2.6** XPS spectra of Nanaoporous gold overlaying Ag% light and dark (A) NP Au 7.5, (C) NP Au 12.5, (E) NP Au 20 and Au% light and dark (B) NP Au 7.5, (D) NP Au 12.5, (F) NP Au 20.

**Table 2.3** XPS results showing atomic Ag% & Au% of nanoporous gold at 7.5, 10, 12.5, and 20 min dealloying times.

| Sample | Atomic Ag % | Atomic Au % |
|---|---|---|
| NP Au – 7.5 min (Dark) | $16 \pm 4\%$ | $84 \pm 4\%$ |
| NP Au - 7.5 min (Light) | $5 \pm 1\%$ | $95 \pm 1\%$ |
| NP Au – 10 min | $15 \pm 4\%$ | $85 \pm 4\%$ |
| NP Au - 12.5 min (Dark) | $11 \pm 2\%$ | $89 \pm 2\%$ |
| NP Au - 12.5 min (Light) | $\sim 4 \pm 1\%$ | $\sim 96 \pm 1\%$ |
| NP Au - 20 min (Dark) | $\sim 4 \pm 0.8\%$ | $\sim 96 \pm 0.8\%$ |
| NP Au - 20 min (Light) | $\sim 2 \pm 0.4\%$ | $\sim 98 \pm 0.4\%$ |

### 2.2.4 Cyclic voltammetry:

Cyclic Voltammetry is one of the mostly widely used techniques to study and characterize redox systems.[28,29] Cyclic voltammetry is commonly undertaken in a three electrode electrochemical cell with a working electrode, reference electrode and auxiliary (counter) electrode. Auxiliary electrodes are inert electrodes (commonly platinum) and reference electrodes (ex., Ag/AgCl and saturated calomel electrode) have a stable potential. Cyclic Voltammetry is acquired by measuring the current that flows between the working electrode and counter electrode upon application of a voltage between the reference electrode and working electrode.

### 2.2.5 Surface area by electrochemical measurements.

All the electrochemical measurements were either performed using a CHI 100 galvanostat/potentiostat or a multichannel potentiostat CHI 1000A (CHI instruments, Austin, Texas, USA), using a Ag/AgCl (0.1 M KCl) fritted reference electrode and Pt auxiliary electrode. Concentrated sulfuric acid (93% w/w) was purchased from Fisher Scientific. For surface area measurements, six electrodes were run simultaneously. All the electrodes were attached to the leads directly without any further attachments.

Surface area measurements were made in 0.5 M sulfuric acid at a scan rate of 0.025 and 0.01 V/s. To define the electrode area, an $1/8^{th}$ inch diameter hole was punched into a piece of Hyde tape. The nanoporous gold electrode was covered with that tape and wrapped with parafilm so that only $1/8^{th}$ inch area was exposed to the electrolyte solution. Two areas were measured: the geometric area from the area of the circle ($A = \pi r^2$, 0.0792 $cm^2$) and the 'real' electrochemical active surface area using cyclic voltammetry. Nanoporous gold electrodes were first oxidized and then reduced in 0.5 M sulfuric acid during a slow scan cyclic voltammetric experiment and the charge required to reduce the gold oxide formed during the oxidation step was measured to obtain the real surface area of the electrode. Using the conversion factor 400 $\mu C/cm^2$, the real electrochemical active surface area was calculated.[30] Figure 2.7 shows the cyclic voltammogram of nanoporous gold and planar gold. For example, the cyclic voltammogram in Figure 2.7 (Nanoporous gold) shows a charge $4.2 \times 10^{-4}$ C required to reduce the gold oxide formed during the oxidation step. Dividing this charge by the conversion factor of 400 $\mu C/cm^2$ yields an electrochemically active surface area 1.05

$cm^2$. The ratio between the real surface area to geometrical area is called the roughness factor.[30] The roughness factor for this electrode is 13.3. Figure 2.8 shows the cyclic voltammograms of nanoporous gold with diiferent dealloying times along with variation in color (dark vs light leaf). Table 2.4 gives the respective surface area and roughness factor values. This data is plotted in Figure 2.9.

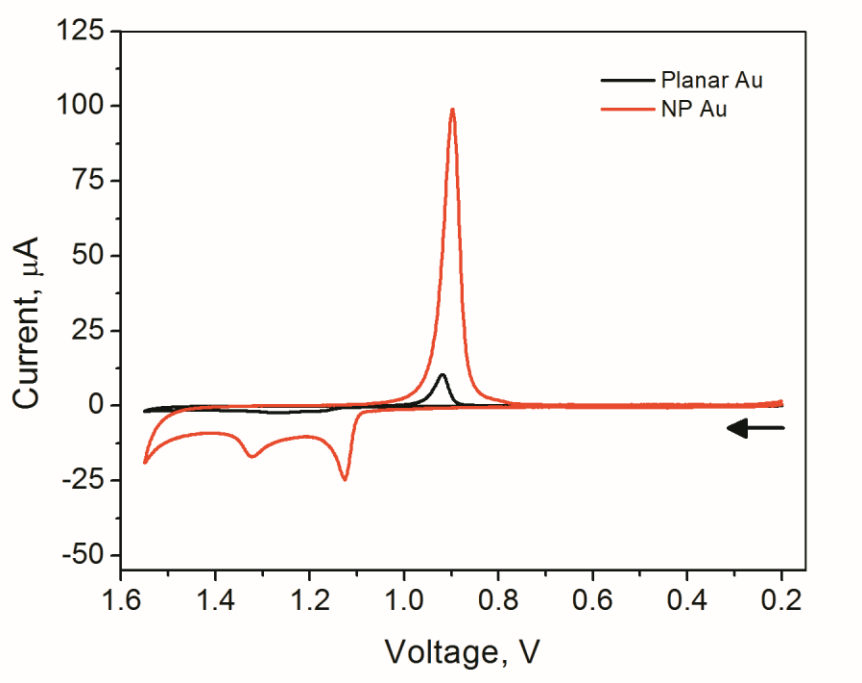


**Figure 2.7** Cyclic voltammetric curves of planar gold and nanoporous gold dealloyed for 12.5 min. Electrolyte: 0.5 M $H_2SO_4$, Scan rate: 100 mV/s

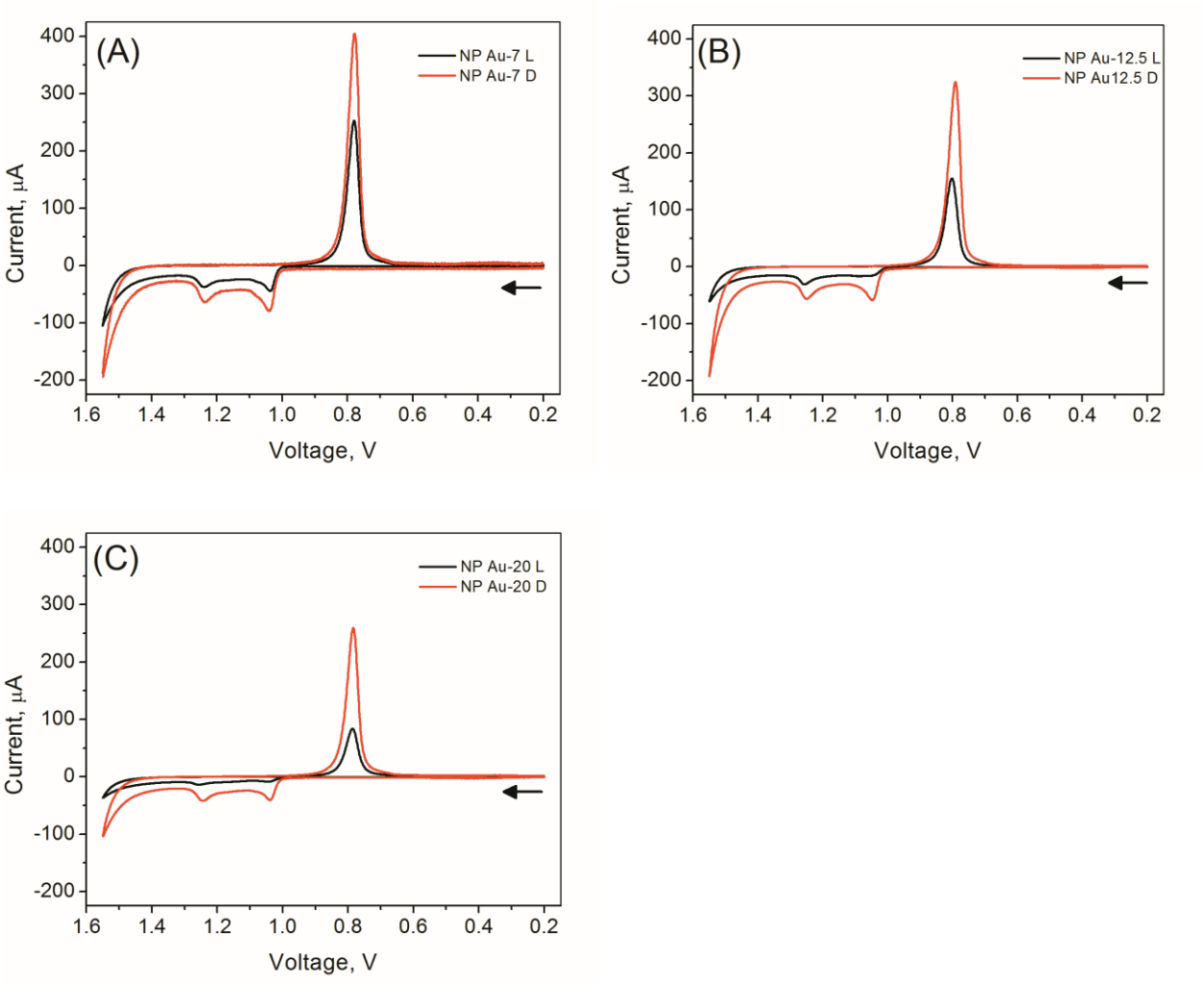


**Figure 2.8** Cyclic voltammetric curves of nanoporous gold (A) Np Au 7.5 dark and light (B) Np Au 12.5 dark and light (C) Np Au 20 dark and light. Electrolyte: 0.5 M $H_2SO_4$, Scan rate: 25 mV/s.

**Table 2.4** Roughness factor of nanoporous gold at 7.5, 12.5, and 20 min dealloying times.

| Electrode | Surface area ($cm^2$) | Roughness factor |
|---|---|---|
| NP Au – 7.5 min (Dark) | 1.9±0.3 | 24± 4 |
| NP Au - 7.5 min (Light) | 1.3±0.4 | 16± 5 |
| NP Au - 12.5 min (Dark) | 2±0.2 | 25 ± 3 |
| NP Au - 12.5 min (Light) | 1.2±0.3 | 15± 4 |
| NP Au - 20 min (Dark) | 1.2±0.2 | 15± 3 |
| NP Au - 20 min (Light) | 0.6±0.4 | 7± 5 |

From the Table 2.4, it can be noted that the dark colored electrodes have the highest surface area compared to the light colored electrodes. NP Au-D 12.5 min gave the highest surface area among other nanoporous gold and this electrode was used for further electrochemical studies.[31] It is also clear that nanoporous gold electrodes have a higher surface area compared to planar gold electrodes.

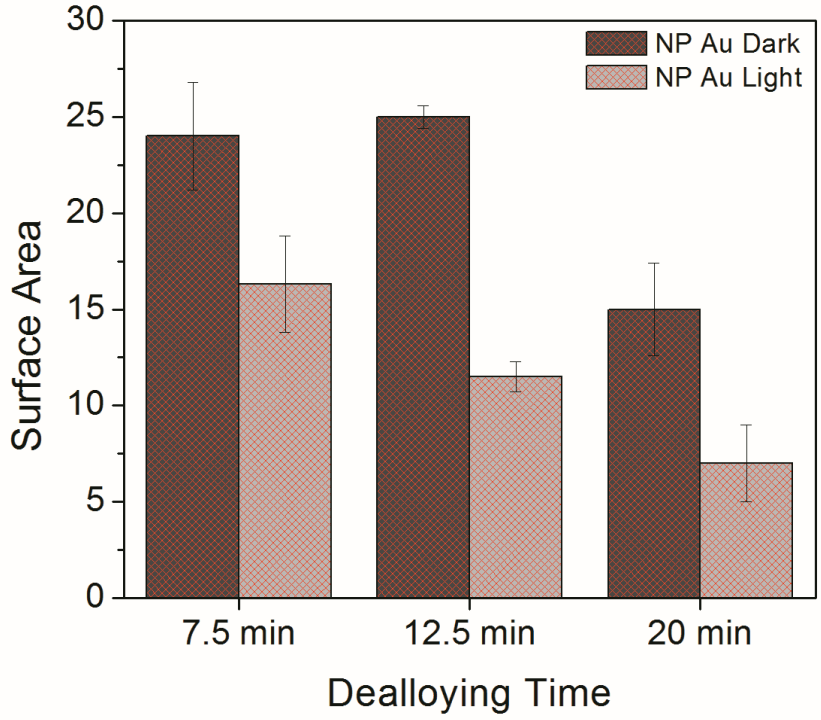


**Figure 2.9** Roughness factor of nanoporous gold at different dealloying times (Dark Vs Light).

### 2.3 Summary of results

The dealloying time in concentrated nitric acid is an important factor in that it controls the porosity of the electrode and its surface area. The dealloying time should be standardized to achieve electrodes with similar porosity and surface area. Dealloying the Ag/Au alloy in nitric acid removes the silver resulting in highly porous structure of gold and is considered as the simplest method to achieve nanoporous gold. EDX and XPS was used to evaluate the silver composition at different dealloying time intervals while SEM images help show the structure and morphological changes as a function of dealloying time.

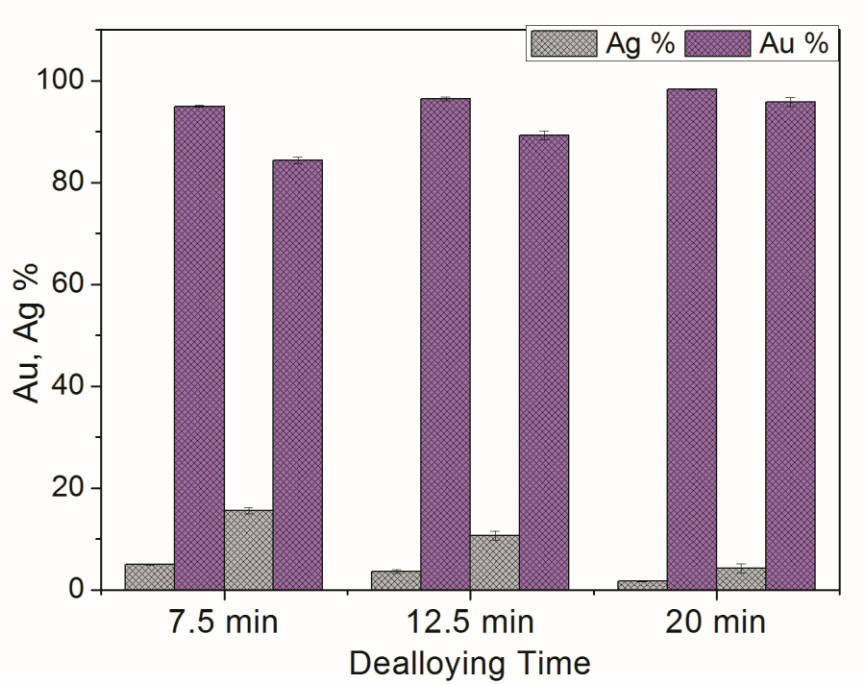


**Figure 2.10** Elemental composition of nanoporous gold from XPS(N=3).

**Table 2.5** Summary of the results: pore size, ligament size, atomic Ag%, surface area of nanoporus gold at 7.5, 12.5, 20 min dealloying times.

| Dealloying time | Pore size (nM) | Ligament size (nM) | Residual Ag (EDX) | Residual Ag (XPS) | Surface area to geo area |
|---|---|---|---|---|---|
| NPG-Dark 7.5 | 5 – 35 | 20 – 50 | | 16$\pm$4% | 24$\pm$ 4 |
| NPG-Light 7.5 | 5 – 50 | 25 – 60 | | 5$\pm$1% | 16$\pm$ 5 |
| NPG-Dark 12.5 | 10 – 40 | 10 -40 | 1$\pm$0.4% | 11$\pm$2% | 25 $\pm$ 3 |
| NPG-Light 12.5 | 15 – 50 | 15 – 50 | 1$\pm$0.4% | 4$\pm$1% | 15$\pm$ 4 |
| NPG-Dark 20 | 20 – 70 | 30 – 70 | | 4$\pm$0.8% | 15$\pm$ 3 |
| NPG-Light 20 | 30 - 100 | 30 -110 | | 2$\pm$0.2% | 7$\pm$ 5 |

# References


1. Walsh, D.; Arcell, L.; Ikoma, T.; Tanaka, J.; Mann, S. Dextran templating for the synthesis of metallic and metal oxide sponges. *Nat. Mater.* **2003***, 2*, 386-390.

2. Lee, D.; Wei, X.; Chen, X.; Zhao, M.; Jun, S. C.; Hone, J.; Herbert, E. G.; Oliver, W. C.; Kysar, J. W. Microfabrication and mechanical properties of nanoporous gold at the nanoscale *Scr. Mater.* **2007***, 56*, 437-440.

3. Shulga, O. V.; Jefferson, K.; Khan, A. R.; D'Souza, V. T.; Liu, J.; Demchenko, A. V.; Stine, K. J. Preparation and Characterization of Porous Gold and its Application as a Platform for Immobilization of Acetylcholine Esterase *Chem. Mater.* **2007***, 19*, 3902-3911.

4. Stine, K. J.; Jefferson, K.; Shulga, O. V. Nanoporous gold for enzyme immobilization *Methods Mol. Biol.* **2011***, 679*, 67-83.

5. Lang, X.; Hirata, A.; Fujita, T.; Chen, M. Nanoporous metal/oxide hybrid electrodes for electrochemical supercapacitors *Nature Nanotechnology* **2011***, 6*, 232 <last_page> 236.

6. Daniel, C. M., Astruc, D. Gold nanoparticles: assembly, supramolecular chemistry, quantum-size-related properties, and applications toward biology, catalysis, and nanotechnology. *Chem. Rev.* **2004,** *104*, 293–234.

7. Wittstock, A.; Biener, J.; Baumer, M. Nanoporous gold: a new material for catalytic and sensor applications *Phys. Chem. Chem. Phys.* **2010***, 12*, 12919-12930.

8. Seo, B.; Kim, J. Electrooxidation of Glucose at Nanoporous Gold Surfaces: Structure Dependent Electrocatalysis and Its Application to Amperometric Detection *Electroanalysis* **2010***, 22*, 939-945.

9. Yu, Y.; Gu, L.; Lang, X.; Zhu, C.; Fujita, T.; Chen, M.; Maier, J. Li Storage in 3D Nanoporous Au-Supported Nanocrystalline Tin *Adv. Mater.* **2011***, 23*, 2443-2447.

10. Ronkainen, N. J.; Halsall, H. B.; Heineman, W. R. Electrochemical biosensors *Chem. Soc. Rev.* **2010***, 39*, 1747-1763.

11. Luppa, P. B.; Sokoll, L. J.; Chan, D. W. Immunosensors—principles and applications to clinical chemistry *Clinica Chimica Acta* **2001***, 314*, 1-26.

12. Chen, L. Y.; Lang, X. Y.; Fujita, T.; Chen, M. W. Nanoporous gold for enzyme-free electrochemical glucose sensors *Scr. Mater.* **2011***, 65*, 17 <last_page> 20.

13. Erlebacher, J. An Atomistic Description of Dealloying *J. Electrochem. Soc.* **2004***, 151*, C614.

14. Erlebacher, J. An Atomistic Description of Dealloying *J. Electrochem. Soc.* **2004***, 151*, C614.

15. Erlebacher, J.; Aziz, M. J.; Karma, A.; Dimitrov, N.; Sieradzki, K. Evolution of nanoporosity in dealloying *Nature* **2001***, 410*, 450-453.

16. Guliants, V. V.; Carreon, M. A.; Lin, Y. S. Ordered mesoporous and macroporous inorganic films and membranes *J. Membr. Sci.* **2004***, 235*, 53-72.

17. Wang, C. H.; Yang, C.; Song, Y. Y.; Gao, W.; Xia, X. H. Adsorption and Direct Electron Transfer from Hemoglobin into a Three-Dimensionally Ordered Macroporous Gold Film *Advanced Functional Materials* **2005***, 15*, 1267-1275.

18. Egerton, R. *Physical Principles of Electron Microscopy: An Introduction to TEM, SEM, and AEM;* Springer Science+Business Media: **2006**.

19. Reimer, L. *Scanning Electron Microscopy: Physics of Image Formation and Microanalysis;* Springer: **1998**.

20. Goldstein, J. *Scanning Electron Microscopy and X-ray Microanalysis: Third Edition;* Springer US: **2003**.

21. Barnes, P. R. F.; Mulvaney, R.; Wolff, E. W.; Robinson, K. A technique for the examination of polar ice using the scanning electron microscope *J. Microsc.* **2002***, 205*, 118-124.

22. Russell, S. D.; Daghlian, C. P. Scanning electron microscopic observations on deembedded biological tissue sections: Comparison of different fixatives and embedding materials *J. Electron Microsc. Tech.* **1985***, 2*, 489-495.

23. Dixon, M. C.; Daniel, T. A.; Hieda, M.; Smilgies, D. M.; Chan, M. H.; Allara, D. L. Preparation, structure, and optical properties of nanoporous gold thin films *Langmuir* **2007***, 23*, 2414-2422.

24. Seker, E.; Reed, M. L.; Begley, M. R. Nanoporous Gold: Fabrication, Characterization, and Applications *Materials* **2009***, 2*, 2188-2215.

25. Watts, J. F.; Wolstenholme, J. In *Electron Spectroscopy: Some Basic Concepts;* An Introduction to Surface Analysis by XPS and AES; John Wiley & Sons, Ltd: 2003; 2005; pp 1-15.

26. Watts, J. F.; Wolstenholme, J. An Introduction to Surface Analysis by XPS and AES **2003**.

27. Moulder, J. F.; Chastain, J. *Handbook of X-Ray Photoelectron Spectroscopy: A Reference Book of Standard Spectra for Identification and Interpretation of XPS Data;* Perkin-Elmer Corporatioon, Physical Electronics Division: **1992**.

28. Bard, A. J., New challenges in electrochemistry and electroanalysis. *Pure & Appl. Chem. ,* **1992***, 64*, 185-192.

29. AnonymousAllen J. Bard and Larry R. Faulkner, Electrochemical Methods: Fundamentals and Applications, New York: Wiley, 2001, 2nd ed. *Russian J. Electrochem.* **2002***, 38*, 1364-1365.

30. Kleijn, S. E. F.; Yanson, A. I.; Koper, M. T. M. Electrochemical characterization of nano-sized gold electrodes fabricated by nano-lithography *J Electroanal Chem* **2012***, 666*, 19-24.

31. Patel, J.; Radhakrishnan, L.; Zhao, B.; Uppalapati, B.; Daniels, R. C.; Ward, K. R.; Collinson, M. M. Electrochemical Properties of Nanostructured Porous Gold Electrodes in Biofouling Solutions *Anal. Chem.* **2013***, 85*, 11610-11618.

# Chapter3: Electrochemical Performance of Nanoporous gold and Open Circuit Potential

## 3.1 Electrochemical studies

Electrochemical measurements were performed using a CHI 100 potentiostat. A Ag/AgCl (3.5 M KCl) reference electrode and a Pt auxiliary electrode were used in conjunction with a multichannel potentiostat (CH 1000A) consisting of six working electrodes, one auxiliary electrode and one reference electrode inserted in a specially made electrochemical cell containing the desired electrolyte solution (redox couple, supporting electrolyte or biofouling solutions). By using the multichannel potentiostat, comparison between multiple working electrodes in one solution was easy and the experiments took less time. Figure 3.1 shows the electrochemical cell connected to the multichannel potentiostat.

**Figure 3.1** Electrochemical setup using the multichannel potentiostat.

## 3.2 Cyclic voltammetry studies of nanoporous gold electrodes in potassium ferricyanide.

Nanoporous gold electrodes dealloyed for 12.5 min were used as working electrodes to acquire CVs in 2 mM potassium ferricyanide/PBS (pH 7) solution at scan rates of 10, 20, 50, 100, 200 mV/s, respectively. Under the conditions used in this work, ferricyanide is reversible redox couple and exchanges electrons quickly with the electrode surface.

In Figure 3.2(A & B), cyclic voltammograms of ferricyanide at sweep rates ranging from 10 mV/s to 200 mV/s are shown for a planar gold electrode and a nanoporous gold electrode. As the scan rate is increased from 10 mV/s to 200 mV/s, the current obtained at each electrode increases and greater peak splitting is being observed. Theoretically, at slow sweep rates, the peak faradaic current should be linearly related to the square root of the sweep rate and the peak splitting (ΔEp) should be 59 mV/n. At 10 mV/s, the peak splitting is 59 mV for ferricyanide at the planar and nanoporous electrode. As can also be seen in Figure 3.2 (C), the peak current is linearly proportional to square root of sweep rate. Results from the regression analysis gave intercept of zero, slope (μAs/V) 3.58 & 2.80 and $R^2$ 0.9997 & 0.9781. At higher scan rates, redox species that are depleted on to electrode surface are less compared to lower scan rates, potential that is applied to the electrode becomes shorter and less redox species are depleted on the surface of the electrode compared to lower scan rates. Even though nanoporous gold has a higher area compared to planar gold

electrodes, all the area is not utilized by redox molecules and smaller currents are seen.

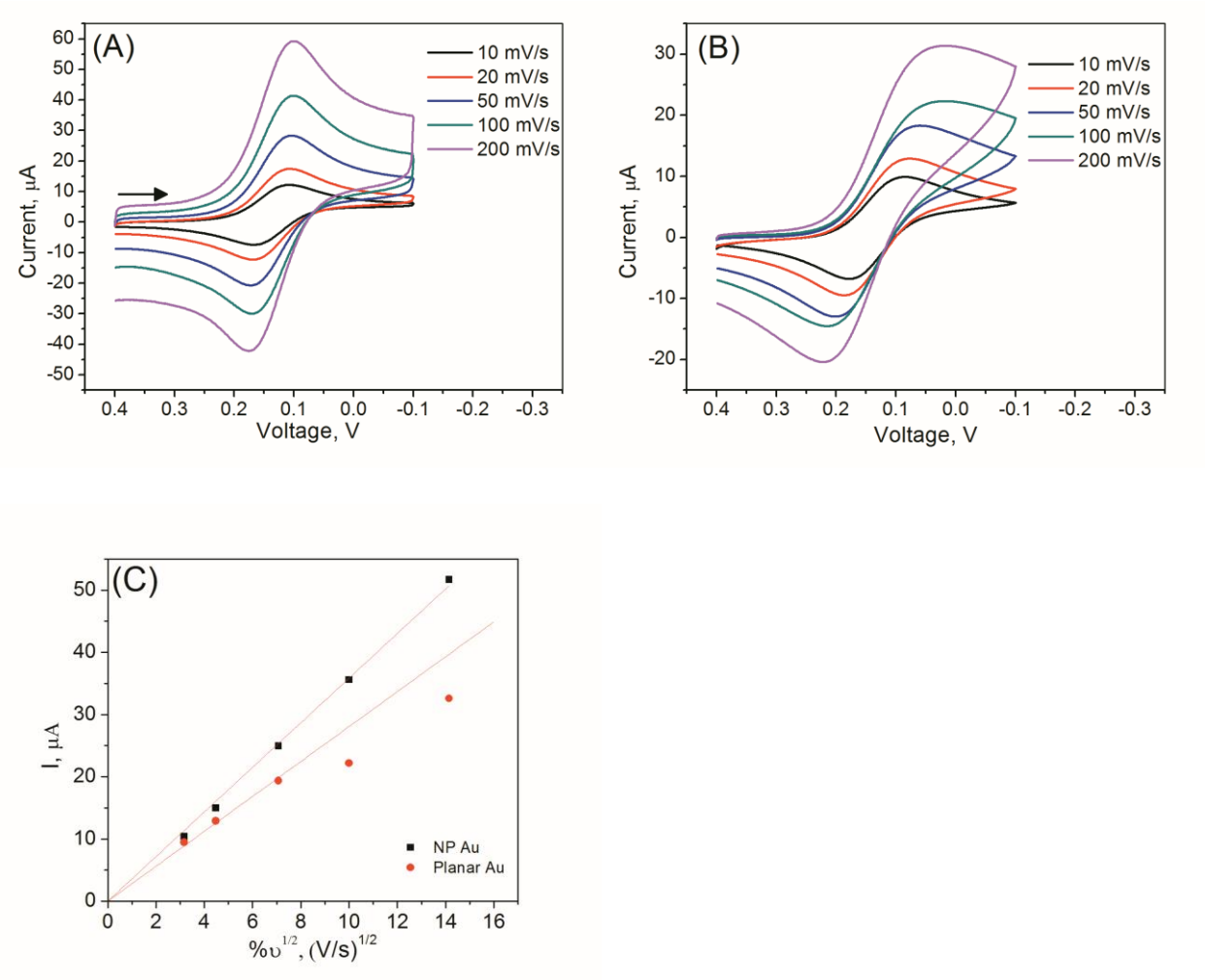


**Figure 3.2** Cyclic voltammetric curves of in potassium ferricyanide ($Fe(CN)_6^{3-}$, 2 mM ) in 0.1 M Phosphate buffer (pH 7)/0.1 M KCl at scan rates 10, 20, 50, 100, 200 mV/s. (A) Nanoporous gold (B). (C) Plot of peak current versus square root of scan rate. The solid lines: linear regression lines.

### 3.3 Performance of electrode in biofouling solutions in buffer.

Nanoporous gold electrodes were used because of their higher surface area, excellent electron transfer and the possibility for reduced biomolecule adsorption on the

electrode surface. Nanoporous gold electrodes dealloyed for 12.5 min were used for the biofouling studies. Comparisons were made to planar gold electrodes. "In this study, we evaluated the electrochemical response of potassium ferricyanide, $Fe(CN)_6^{3-}$, at nanoporous gold electrodes and planar gold electrodes in the presence of biofouling agent like (bovine serum albumin, BSA). BSA is a globular protein with a molecular weight of ~ 66 KDa and size (14 x 4 nm)[1] and considered as major protein in blood plasma. The premise behind these experiments is it helps us to know if albumin adsorbs on the surface of the electrode and thus hampers the electrochemical response (electron transfer) of redox molecule in solution. When the electrodes come in contact with biological solutions, proteins like albumin and fibrinogen adsorb on the electrode and hinder the electrochemical response. This can be seen in cyclic voltammetric experiment if the peak splitting (ΔEp) is larger and the current decreases for a redox molecule in a solution containing the protein.

Unless otherwise noted, in these experiments, UV-cleaned nanoporous gold electrodes prepared using a 12.5 min dealloying time and planar Au (UV-cleaned) electrodes were placed in a solution of potassium ferricyanide ($Fe(CN)_6^{3-}$, 2mM, pH 7.2 ) and a cyclic voltammogram was collected at scan rate 100 mV/s. Bovine serum albumin (BSA, 2mg/mL) was added to the solution and CVs were collected over the course of an hour. The data shown in Figure 3.3 were collected at distinct intervals of time after addition of BSA: ~ 1, 2, 5, 10, 15, 20, 30, 40, 50, 60 min.

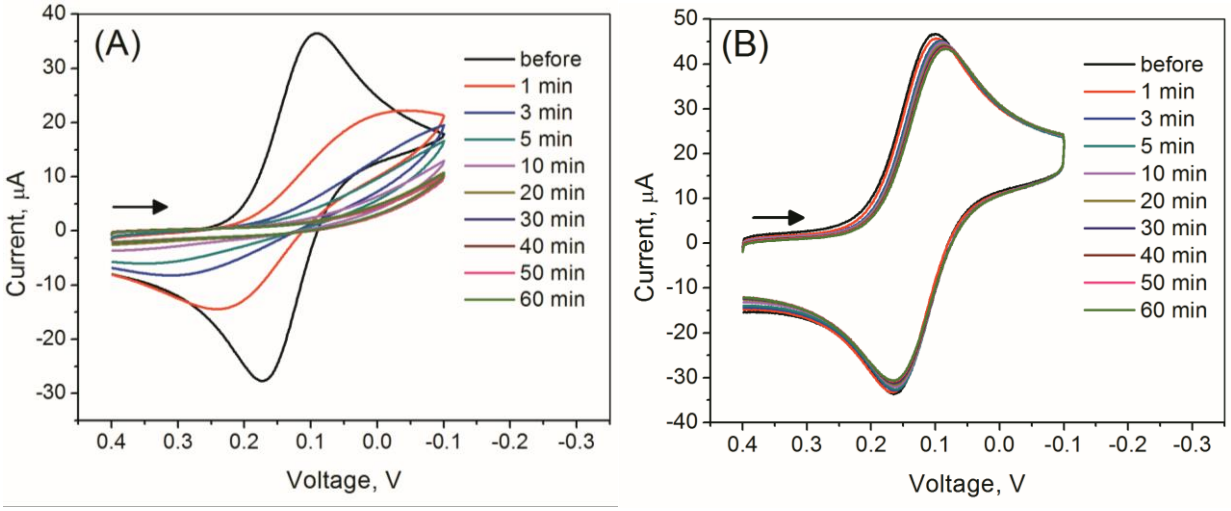


**Figure 3.3** Cyclic voltammetric (CV) curves obtained at (A) nanoporous gold, (B) planar gold electrodes in potassium ferricyanide ($Fe(CN)_6^{3-}$, 2mM ) in 0.1 M Phosphate buffer (pH 7)/0.1 M KCl before and after addition of bovine serum albumin (2 mg/mL). Scan rate: 100 mV/s. CVs were acquired over a 60 minute period.

Initially, before addition of BSA, the voltammetric peak shape observed at both the electrodes (planar Au and nanoporus Au) corresponds to a diffusion-controlled, reversible redox probe freely exchanging electrons with the electrode surface. After addition of BSA, the current decreases, ΔEp increase, and the shape of the voltammetric curve becomes less peaked shaped and more 'flatter' indicative that BSA is adsorbing on the electrode surface and interfering with electron transfer. Planar gold electrodes also showed similar response towards exposure to human serum albumin and immunoglobulin G.[2-8] The extent of these changes depends on the electrode. At an as-received planar gold electrode, the current dropped significantly faster and the voltammetric shape changed quickly within five minutes compared to nanoporous gold

electrodes. Within ~ 10 minutes of the planar gold electrodes being in solution, these electrodes were rendered essentially irresponsive to $Fe(CN)_6^{3-}$. The best results were observed for nanoporous gold electrodes with little drop in current over a longest time (~ 22 hours).

Additional studies were carried out on nanoporous gold electrodes with slightly different pore sizes. Nanoporous gold electrodes (dealloyed for 12.5 min NP: Au-12.5 Dark, Light) with slightly different pore size and surface area were made by changing the dealloying conditions, mainly its exposure to nitric acid. The CV response for $Fe(CN)_6^{3-}$ following exposure to BSA is shown in Figure 3.4. Nanoporous gold with larger pore sizes and smaller surface area (NP AU- 12.5 Light) having a ratio of real-to-geometric area of 15 ± 1 showed a larger drop in the current and change in peak splitting while nanoporous gold with a smaller pore size and larger surface area (NP AU-12.5 Dark) and a high real-to-geometric area ratio of 25 ± 3 exhibited almost no change in the cyclic voltammetric response over the course of an hour.

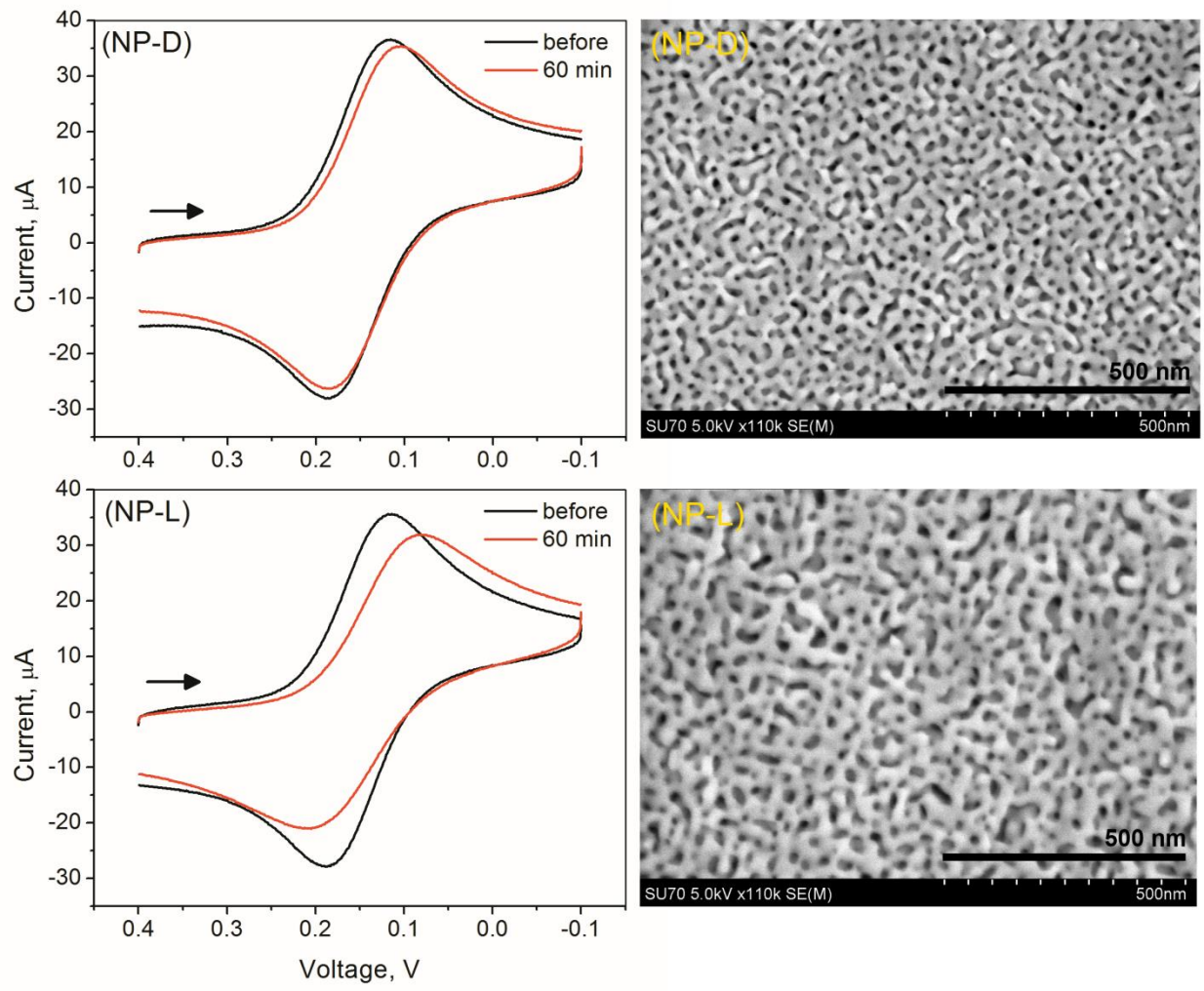


**Figure 3.4** Left: Cyclic voltammetric (CV) curves obtained at nanoporous gold electrodes in potassium ferricyanide ($Fe(CN)_6^{3-}$, 2mM ) in 0.1 M Phosphate buffer (pH 7)/0.1 M KCl before and after addition of bovine serum albumin (2 mg/mL). Scan rate: 100 mV/s. CVs were acquired over a 60 minute period. Representative SEM images of nanoporous gold with two different surface area ratios: 25 for NP dark and 16 for NP light.

To more quantitatively evaluate the electrodes, the normalized current was plotted as function of time after the addition of BSA to the solution of potassium ferricyanide. The data shown in the Figure 3.5 were normalized by dividing the

Faradaic current at ~ 100 mV following the addition of BSA by the current measured immediately before the addition of BSA. For all the electrodes, the normalized peak current decreased, the extent of which was strongly dependent on the morphology of the electrode. The time it took for the current to drop one half of its value was three minutes for planar gold. In contrast, for nanoporous gold with the smaller surface area (NP Au 12.5 min Light), an average drop in current of 12 ± 8% was observed after 60 minutes. For NP Au 12.5 min Dark, however, the current drop was small (5 ± 3%) and ~ 95 % of the original Faradaic current was still observed one hour after the addition of BSA. Nanoporous gold outperformed the planar gold electrodes. Nanoporous gold electrodes (NP Au 12.5 min dark) with surface area 15 showed reduced performance compared to NP Au 12.5min Light. Nanoporous gold with smaller pore size and high surface area performed better in the presence of biofouling agents like BSA and it took longer time for BSA to cover the entire surface of the electrode.

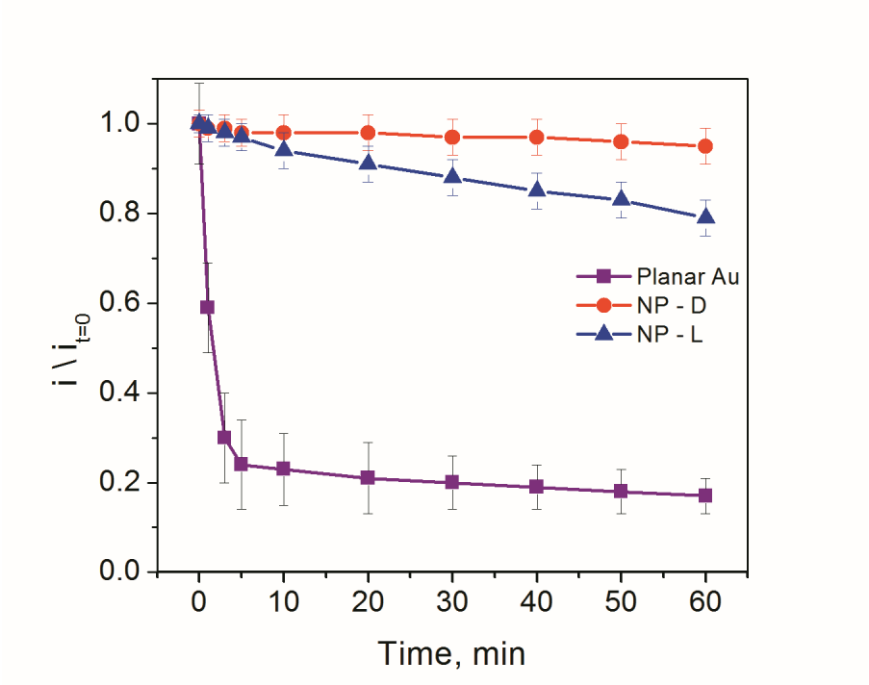


**Figure 3.5** Normalized current before (t=0) and after addition of 2 mg/mL of BSA to solution for the nanoporous gold dark (red circle), nanoporous gold light (blue triangle), planar gold (purple square) at ~ 100 mV. Error bars represent the standard deviations obtained from 3-4 electrodes.

The peak splitting, ΔEp, is related to the kinetics of electron transfer and is sensitive to the cleanliness of the electrode surface. For both nanoporous gold dark and light, the peak splitting for potassium ferricyanide is plotted against time following addition of BSA. A blocked surface exhibits a slow rate of electron transfer resulting in decreased peak current and increased in peak splitting. Figure 3.6 shows how ΔEp of potassium ferricyanide changes over a course of hour after addition of BSA for both nanoporous gold electrodes. As can be seen in the Figure 3.6, ΔEp increases more for the light colored electrode than for the dark color electrode. From these results, it can

be seen that a pore size dependence is present. Nanoporous gold electrodes with smaller pore size are more successful in being able to study the electrochemistry of redox couple in a solution containing BSA compared to light colored electrode and planar gold which showed complete passivation in shorter time.

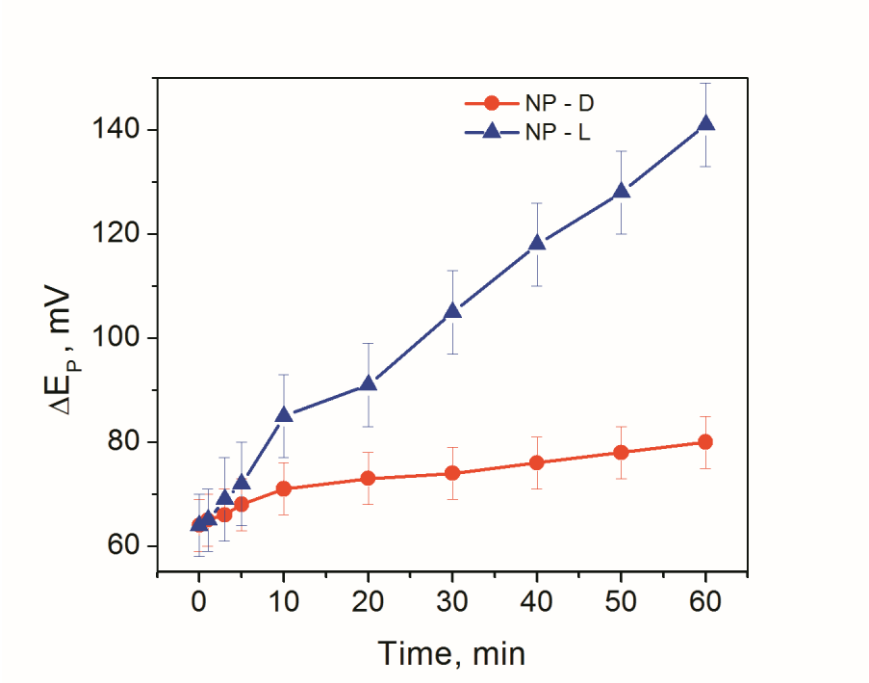


**Figure 3.6** Plot of ΔEp for nanoporous gold dark (blue triangle) and light (red circle) before and after the addition of BSA (concentration: 2 mg /mL). The cyclic voltammetric data is shown in Figure 3.4.

Electrode porosity plays a crucial role in the observed electrochemistry. The possible reasons for why electrode porosity is so important are: (1) Mass transport limitations prevent BSA from reaching the inner surface on the time scale of the experiment. (2) The porosity and nanoscale architecture of nanoporous gold electrodes make the blocking of the surface by protein adsorption and unfolding less effective. (3) The higher surface area of the porous electrodes provide plenty of sites for electron

transfer to take place even in the presence of adsorbed protein".[2] Possible explanation of the longer passivation process for nanoporous gold is shown in the Figure 3.7.

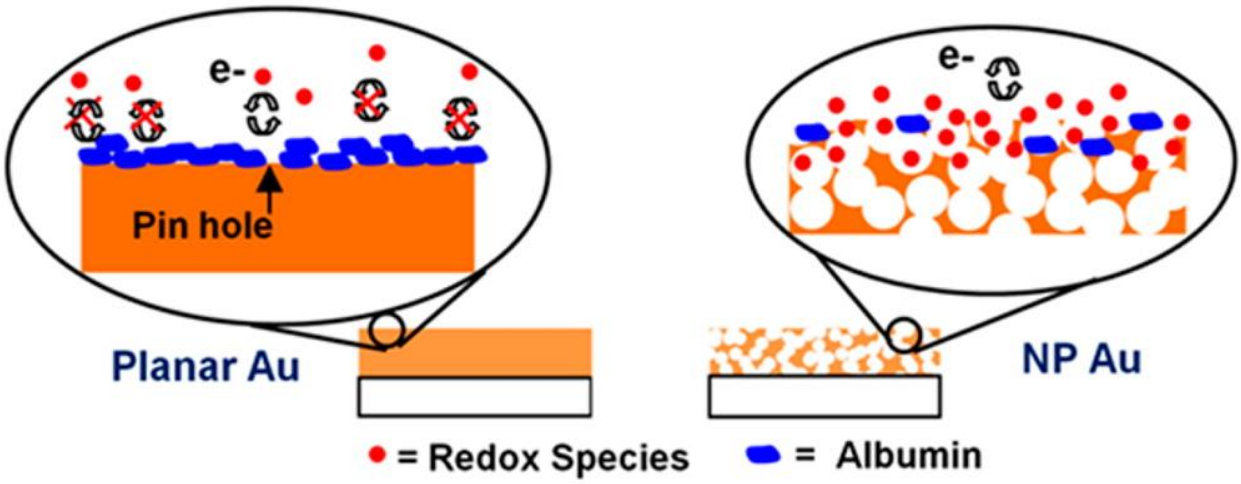


**Figure 3.7** Simplified cartoon of the surface of nanoporous gold and planar gold in the presence of albumin and a small redox molecule in the solution. Electron transfer is hindered at planar gold but not at nanoporous gold. Reprinted with permission from Jay Patel; Logudurai Radhakrishnan; Bo Zhao; Badharinadh Uppalapati; Rodney C. Daniels; Kevin R. Ward; Maryanne M. Collinson; *Anal. Chem.* **2013,** 85, 11610-11618. Copyright 2013, American Chemical Society.

### 3.4 Performance of the electrodes in blood and serum.

In these experiments, nanoporous gold electrodes (Dark) prepared by 12.5 min dealloying time (UV-cleaned) along with planar Au (UV-cleaned) electrodes were used. To evaluate the performance of the electrodes in biologic solutions, potassium fericyanide ($Fe(CN)_6^{3-}$, 2mM ) was doped into a serum sample and heparinized blood. Cyclic voltammograms were collected at scan rate 100 mV/s over the course of an hour.

The data shown in Figure 3.8 shows the cyclic voltammetric curve of $Fe(CN)_6^{3-}$ in serum and blood at nanoporous gold electrode after ~ 60 minutes in solution.

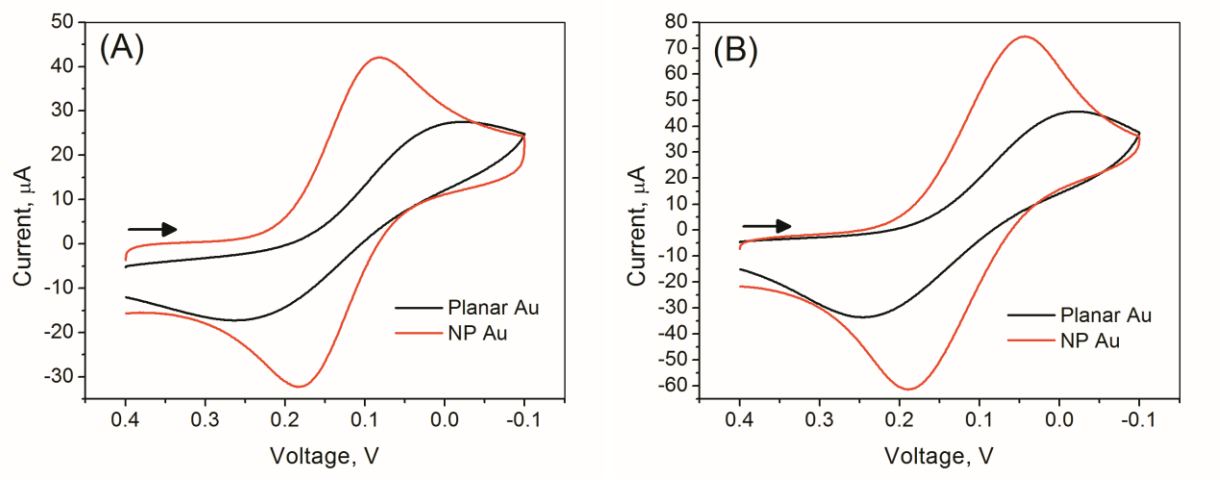


**Figure 3.8** CVs acquired at nanoporous gold and planar gold after 60 minutes in human serum and heparinized pig blood doped with $Fe(CN)_6^{3-}$. Scan rate: 100 mV/s

Initially, before immersing the electrodes in serum and blood, CV's were taken in buffer with potassium ferricyanide ($Fe(CN)_6^{3-}$, 2mM ), the voltammetric peak shape observed at both the electrodes (planar Au and Nanoporous Au) corresponds to a diffusion-controlled, reversible redox probe freely exchanging electrons with the electrode surface. After the electrodes were immersed in potassium ferricyanide ($Fe(CN)_6^{3-}$, 2mM) doped into a serum sample and heparinized blood, the shape of CVs at the planar electrode quickly changed from diffusion controlled in buffer to sigmoidal shape in serum and blood. However, the shape of nanoporous gold did not change significantly. As can be seen, the current decreases for the nanoporous gold electrode in serum and blood, while peak splitting ΔEp is 75 mV. For planar gold electrodes, the peak splitting ΔEp increases to 270 mV. Nanoporous gold electrodes out-performed

planar gold in both biological samples (serum and blood). The redox activity of ferricyanide was retained.

### 3.5 Oxidation-Reduction potential (ORP)

Oxidation-reduction potential (ORP), often referred to as zero current potential or open circuit potential (OCP), is the potential of an inert electrode with respect to a reference electrode in a given medium under zero current conditions.[9] Many important factors contribute to measured value of ORP including. [9]

i) Concentrations (activities)

ii) Redox species present in the system

iii) Rate at which electrons transfer between a redox species and electrode.

The rate of electron exchange is a vitally important characteristic of the electrode as it ultimately determines what redox species are being detected and the time needed to reach "steady-state" or equilibrium.[10-12] An oxidation-reduction system (redox couple), consisting of both oxidized and reduced species that are present in appreciable concentrations in a medium, where electrons transfer takes place from reductant to an oxidant which can undergo the below reaction

$$\mathrm{Ox} + n\mathrm{e}^- \longrightarrow \mathrm{Red}$$

where Ox is the oxidized form, $n\mathrm{e}^-$ is the number of electrons transferred in the reaction and Red is reduced form. The potential measured is related to the concentration (activities) of oxidants and reductants as described by the Nernst equation.

$$\mathrm{E} = \mathrm{E}_0 - \frac{0.0591}{\mathrm{n}} \log \left\{ \frac{\mathrm{C\ (Red)}}{\mathrm{C}\ (Ox)} \right\}$$

where E is the measured potential (with respect to a reference), $E_0$ is the standard reduction potential of the redox couple, 0.0592 is the value of [2.303(RT/F)] at 25°C (R is the gas constant and F is Faraday's constant), *n* is the number of electrons transferred, $C_{Red}$ and $C_{Ox}$ are the concentrations of the reduced and oxidized forms of the redox couple, respectively. ORP is a measure of the electron transfer between the total oxidants and reductants in the medium and dependent on the total concentrations (activities)[10-12].

### 3.6 ZoBell's solution

ZoBell's solution is a 0.1 molar KCl solution containing equimolal amounts of $K_4Fe(CN)_6$, and $K_3Fe(CN)_6$ and was developed by Zobell in 1946.[13] It is used us a standard solution for calibrating redox measurements. E(Redox) of a sample relative to Ag/AgCl is determined by measuring the E(Redox)of both sample and standard (ZoBell's solution) at the same temperature. Calibration of reference electrode is crucial step in measuring the open circuit potential (OCP) of biologic solutions.

### 3.7 Instrumentation and blood samples

Electrochemical measurements (OCP) were performed using a CHI 100 potentiostat and a silver chloride coated silver wire as the reference electrode and nanoporous gold prepared by 12.5 minutes dealloying in nitric acid. Blood samples were obtained under the collaboration of Dr. Rodney C. Daniels, Dr. Penny Reynolds and the Division of Animal Research at VCU. Human blood samples were obtained under collaboration of Dr. Rodney C. Daniels. For these samples, an Autolab potentiostat was used for measuring the ORP of three nanoporous gold electrodes at a time. Three

nanoporous electrodes and one reference electrode were inserted in a specially made electrochemical cell containing the desired solution (blood, plasma or ZoBell's solutions). Electrochemical comparison between various electrodes was easy and the experiments took less time by measuring the OCP of all three electrodes with respect to a single reference electrode simultaneously using Autolab potentiostat. For all other experiments, the CHI potentiostat was used, which can measure the OCP of only one electrode at a time.

### 3.8 OCP of Rabbit Blood and plasma

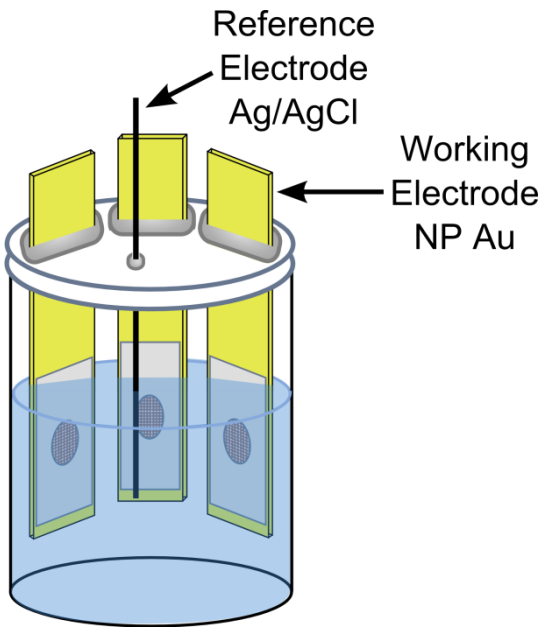


**Figure 3.9** A three electrode electrochemical setup for measuring OCP.

Rabbit blood was collected in sodium heparinized tubes and plasma was separated by centrifugation as needed. OCP measurements were made using a nanoporous gold electrode (prepared by dealloying for 12.5 min) or UV-cleaned planar gold and a AgCl coated Ag reference electrode connected to a CH instrument potentiostat. The three nanoporous gold electrodes along with the reference electrode were immersed in the sample (see Figure 3.9) and the OCP was recorded for 9 minutes for the first gold electrode. The lead to the potentiostat was then connected to the second electrode and the OCP measured for one minute. When finished, the lead was connected to the third electrode and the OCP measured for one minute. Representative raw data is shown in Figures 3.10 while Table 3.1 summarizes the results of OCP measurement at the nanoporous gold and planar gold electrodes in Rabbit blood or plasma. The OCP values at both the planar gold and nanoporous gold electrodes are

different from each other and there is variability from day to day due to different constituents present in blood and plasma. The reference electrode was calibrated using standard ZoBell's solution and the values are given in Table 3.1.

**Table 3.1** OCP of nanoporous gold and planar gold in Rabbit blood and plasma and OCP difference between nanoporous and planar gold. N=3

| Date | NP Au (mV) | Planar Au (mV) | Difference (mV) | Calibration[a] (mV) |
|---|---|---|---|---|
| **Oct-17 (Plasma)** | -119.4 ± 4.3 | -163.1 ± 3.7 | 44 | Np: 142.9<br>Planar: 144.2 |
| **Oct-24 (Blood)** | -105.4 ± 3.2 | -169.1 ± 3.4 | 63 | Np: 144<br>Planar: 142.5 |
| **Oct-31 (Blood)** | -105.1 ± 3.4 | -166 ± 3.0 (N=2) | 61 | Np: 144.2<br>Planar: 142.9 |
| **Nov-2 (Blood)** | -109.1 ± 4 | -169.3 ± 2.1 | 60 | Np: 136.6<br>Planar: 142.4 |
| **Nov-5 (Blood)** | -105.6 ± 4.8 | -163 ± 1.3 (N=2) | 57 | |
| **Nov-7 (Blood)** | -116.6 ± 2.5 | -176.8 ± 4.2 | 60 | Np: 147.5<br>Planar: 151.2 |
| **Nov-9 (Blood)** | -122.9 ± 5.7 | -202 ± 7.9 | 79 | Np: 151.2<br>Planar: 143.3 |
| **Nov-12 (Blood)** | -104.6 ± 3.5 | -158.9 ± 1.7 | 54 | Np: 148.4<br>Planar: 139.8 |
| **Nov-16 (Blood)** | -117.3 ± 2.2 | -157.5 ± 5.8 (N=2) | 40 | Np: 148.6 |

[a] ZoBell's solution

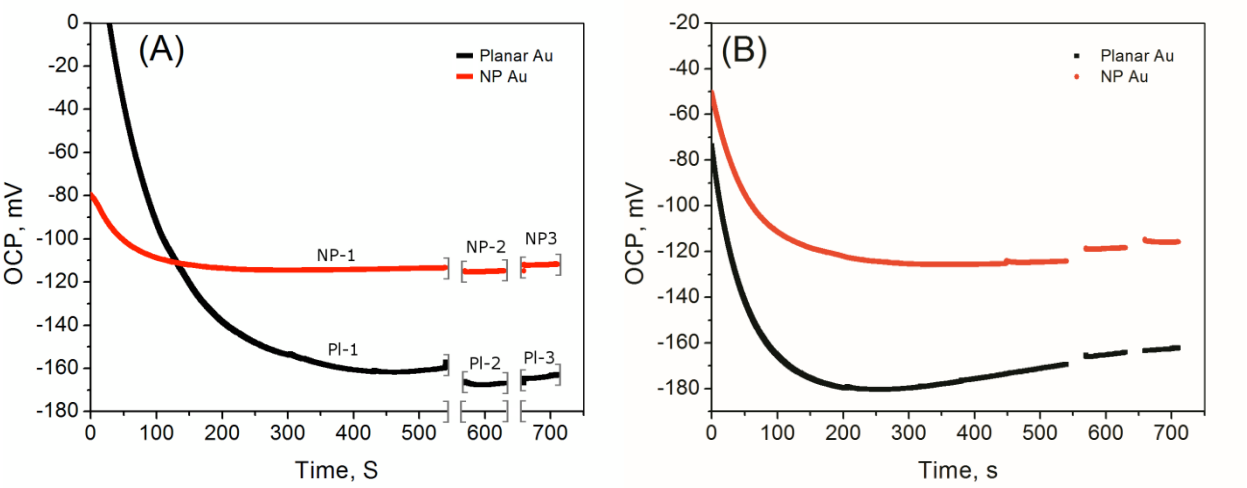


**Figure 3.10** OCP of nanoporous gold and planar gold in (A) Rabbit blood, (B) Rabbit plasma

### 3.9 OCP of Pig blood and plasma

Representative raw data is shown in Figures 3.11 while Table 3.2 summarizes the results of OCP measurement at the nanoporous gold and planar gold electrodes in pig blood or plasma. OCP measurements of both the electrodes are different from each other and there is variability from day to day as observed for the rabbit blood.

**Table 3.2** OCP of nanoporous gold and planar gold in Pig blood and plasma and OCP difference between nanoporous and planar gold. N=3

| Date | NP Au (mV) | Planar Au (mV) | Difference (mV) | Calibration[a] (mV) |
|---|---|---|---|---|
| **Nov-28 Pig Blood,** | -107.9 ± 6.6 | -151.5 ± 2.3 | 44 | NP Au: 145.9<br>Planar Au: 146.2 |
| **Plasma** | -103.8 ± 3.6 | -129.1 ± 5.4 | 25 | |

[a] ZoBell's solution

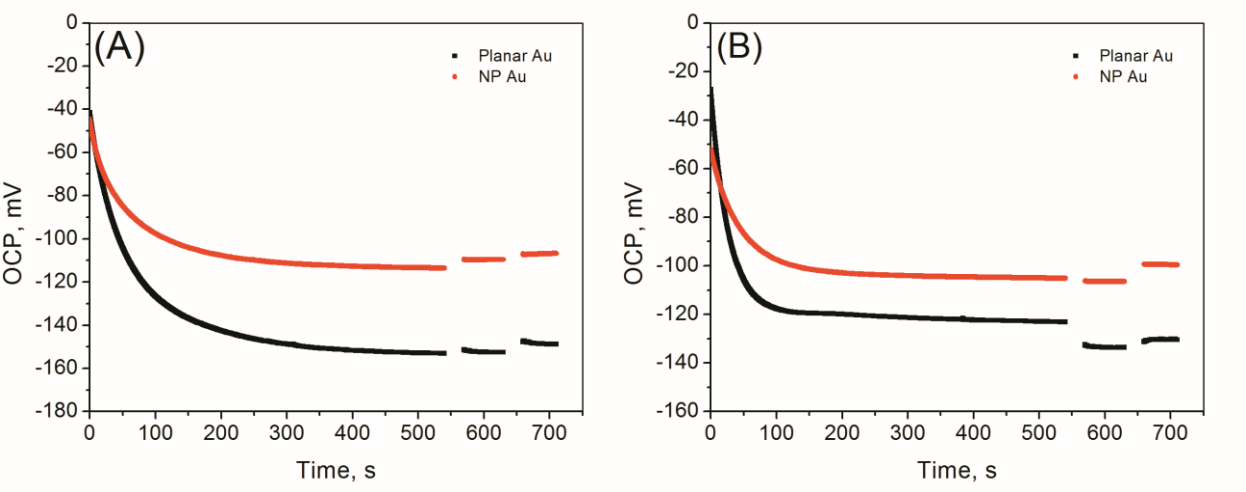


**Figure 3.11** OCP in mV of nanoporous gold and planar gold in (A) Pig blood, (B) Pig plasma

### 3.10 OCP of Rabbit plasma and crashed Rabbit plasma.

To further investigate OCP under different conditions, once when an animal was in a good condition, blood was taken out and then another sample of blood was taken after injuring the animal during shock experiments, just before the animal was going to die (e.g., a crashed Rabbit). Blood was collected from the Rabbit at both intervals in sodium heparinized tubes. Table 3.3 shows the results of OCP of nanoporous gold electrodes in Rabbit Blood. Figure 3.12 shows the OCP of Rabbit plasma at both electrodes. Both OCP measurements are different from each other indicating a difference in the OCP showing significance that OCP helps in measuring the animal condition.

**Table 3.3** OCP of nanoporous gold and planar gold of Rabbit and crashed Rabbit plasma and OCP difference of nanoporous and planar gold. N=3

| Date | NP Au (mV) | Planar Au (mV) | Difference (mV) |
|---|---|---|---|
| **June-27 (Rabbit plasma)** | -119.6 ± 3.6 | -155.5 ± 3.6 | 36 |
| **June-29 (Crashed Rabbit)** | -97.58 ± 3.6 | -128.4 ± 3.6 | 30 |

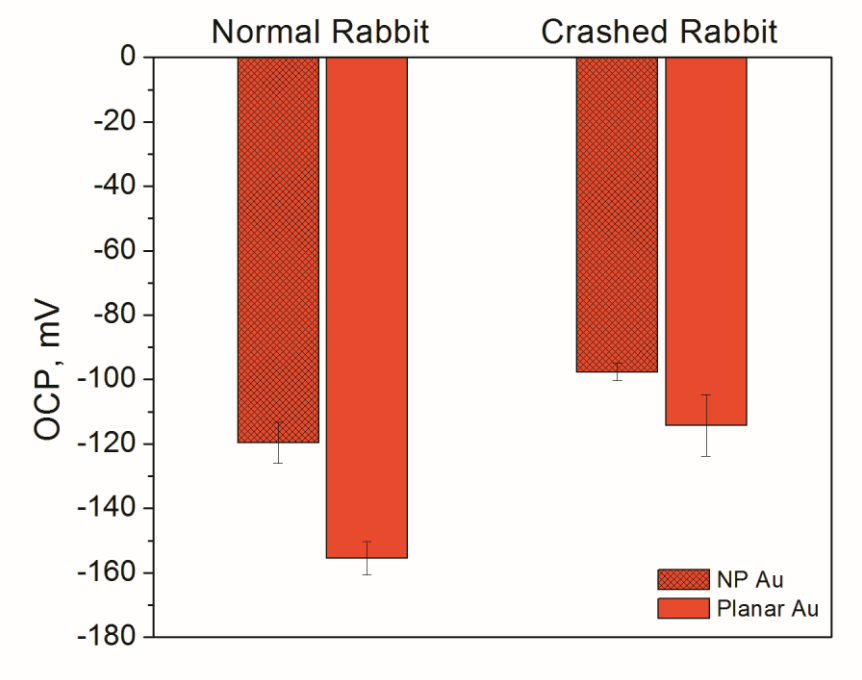


**Figure 3.12** Bar graph shows OCP in mV of nanoporous gold and planar gold for normal Rabbit and crashed Rabbit blood. Error bars represent the standard deviations obtained from 3 electrodes.

### 3.11 OCP of Arterial and Venous blood samples of Rabbit and Pig.

Arterial and venous blood sample were collected from a Rabbit and a Pig. Arterial blood is considered as oxygenated blood and bright red in color, venous blood is considered as deoxygenated blood and dark red in color. To investigate OCP of both arterial and venous blood, both blood samples were collected near the same time. Table 3.4 shows the results of OCP of nanoporous gold electrodes in Rabbit and Pig blood. Both OCP measurements are different from each other indicating a difference in the OCP between venous and arterial blood. Venous blood is having less number of oxygen species compared to arterial blood as it is deoxygenated blood and has a more negative OCP compared to the arterial blood. Figure 3.13 shows the OCP of arterial blood and venous blood of Rabbit and Pig.

**Table 3.4** OCP of nanoporous gold in Pig and Rabbit arterial or venous blood and the OCP difference between arterial and venous blood.

| Date | Np Au (mV) | | Difference (mV) |
|---|---|---|---|
| **Sep-27** | -97 ± 5.2 | (N=4) Arterial Blood | 54 |
| **(Pig)** | -151.1 ± 2.28 | (N=4) Venous Blood | |
| **June-29** | - 100.5 ± 2.7 | (N=3) Arterial Blood | 20 |
| **(Rabbit)** | -120.1 ± 4.5 | (N=3) Venous Blood | |

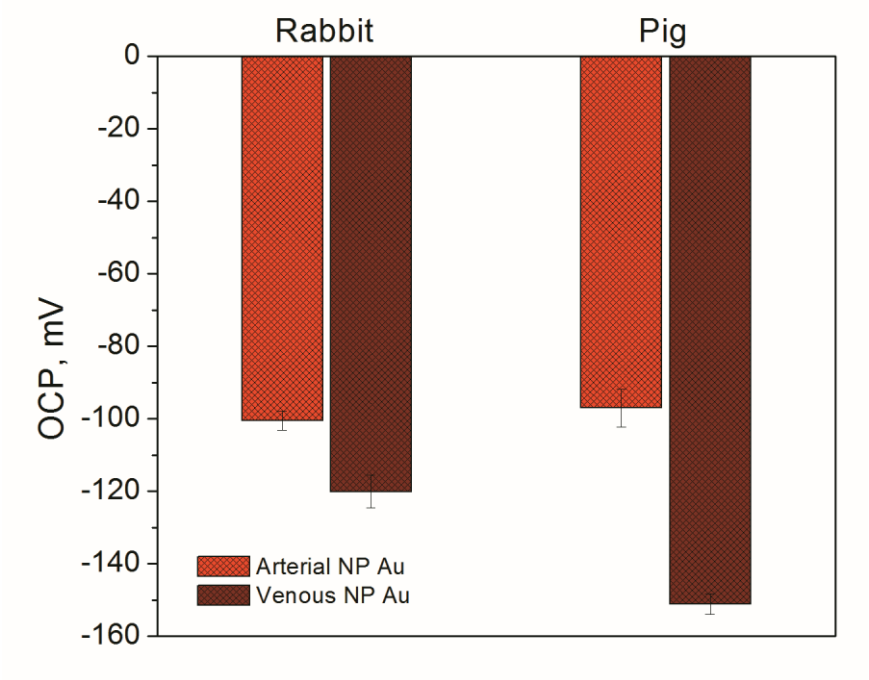


**Figure 3.13** Bar graph shows OCP in mV of nanoporous gold in Rabbit and Pig arterial and venous blood. Error bars represent the standard deviations obtained from 3 electrodes.

### 3.12 OCP of stored Pig blood.

Arterial pig blood was collected stored in sodium heparinized tubes and stored in a freezer at $-4^0$ C. Blood settled when stored in the freezer. As a result, when blood was taken out it was vortexed before testing. OCP was recorded from Day1 to Day10.

Three nanoporous gold electrodes were recorded and compared to planar gold. Table 3.5 shows the results of OCP of nanoporous gold and planar gold electrodes in aged Pig blood. Figure 3.14 shows OCP in mV of nanoporous gold in aged Pig blood from day 1 - 10. Both OCP measurements are different from each other, the difference in the OCP showing significance that blood is changing with time, even though stored in freezer. The difference between the nanoporous and planar gold was 44 mV on the first day and on day 3-10 it was 13-20 mV. Active species that are present on the first day when the sample was collected were inactive within 2 days and OCP had a similar value from day 3-10. The data shows there is an oxidative environment in the stored blood product and increases with time. This shows the potential has significance with age of blood.

**Table 3.5** OCP of nanoporous gold and planar gold in stored Pig blood and OCP difference of nanoporous and planar gold. N=3.

| Date | NP Au (mV) | Planar Au (mV) | Difference (mV) | Calibration[a] (mV) |
|---|---|---|---|---|
| **Nov-28** | -107.9 ± 6.6 | -151.5 ± 2.3 | 44 | Np: 146.2<br>Planar: 145.9 |
| **Nov-30** | -99.1 ± 3.2 | -114.9 ± 5 | 16 | Np: 144.5<br>Planar: 147.1 |
| **Dec-3** | -95.6 ± 3.6 | -114.2 ± 2 | 19 | Np: 144<br>Planar: 148.9 |
| **Dec-5** | -95.3 ± 3.3 | -108.3 ± 1.3 | 13 | Np: 138.2<br>Planar: 144 |
| **Dec-7** | -91.3 ± 5.2 | -110.9 ± 4 | 20 | Np: 130.4<br>Planar: 135.5 |

[a] ZoBell's solution

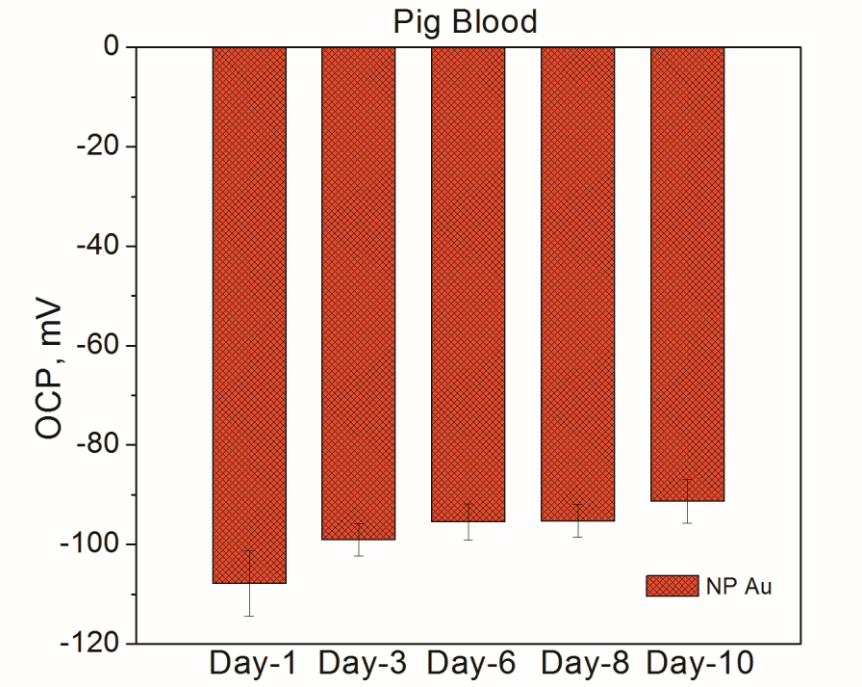


**Figure 3.14** Bar graph shows OCP in mV of nanoporous gold in stored Pig blood from day 1 - 10. Error bars represent the standard deviations obtained from 3 electrodes.

### 3.13 OCP of different animals and human.

Baseline blood (fresh blood of a healthy species) was collected from a Rat, a Rabbit, a Monkey and humans (male and female). OCP were measured with a nanoporous gold electrode and Ag/AgCl electrode connected to a CHI potentiostat. One electrode was measured at a time. Human blood was evaluated using the Autolab potentiostat which allowed three electrodes to be tested at same time. The electrodes were immersed in blood and the OCP was recorded for ~10 minutes. Table 3.6 and Table 3.7 show the results of OCP of nanoporous gold electrodes in different animals and humans. Figure 3.15 and Figure 3.16 shows OCP in mV of nanoporous gold in different animals and humans. Both OCP measurements are different from one other indicating difference in the OCP of animals. It is showing significance that different animals and humans have different OCP. As various oxidation and reduction reactions are taking place in each individual species, it is definite to have different OCP.

**Table 3.6** OCP of nanoporous gold in different animals (Rat, Rabbit, Monkey), Humans (Male, Female). N=3.

| | **Rat (mV)** | **Rabbit (mV)** | **Monkey (mV)** | **Human (mV) (Male)** | **Human (mV) (Female)** |
|---|---|---|---|---|---|
| **Np Au** | -70.2 ± 4.9 | -76.5 ± 2.7 | -98.6 ± 4.2 | -133.6 ± 6.9 | -120.2 ± 5.2 |

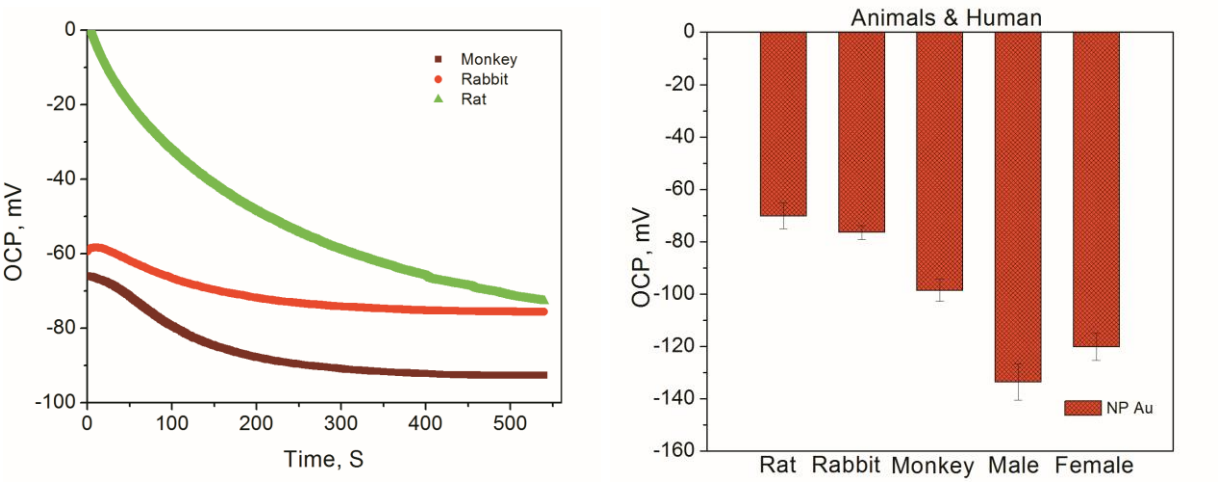


**Figure 3.15** OCP in mV of nanoporous gold in different animals Rat, Rabbit, Monkey. Right bar graph shows OCP of nanoporous gold in different animals (Rat, Rabbit, Monkey), Humans (Male, Female). Error bars represent the standard deviations obtained from 3 electrodes.

**Table 3.7** OCP of nanoporous gold in different animals (Pig, Sheep, Rabbit blood (arterial and venous))

| | **Pig Blood (mV)** | **Sheep Blood (mV)** | **Rabbit Arterial blood (mV)** | **Rabbit Venous blood (mV)** |
|---|---|---|---|---|
| **Np Au** | -101.8 ±7.3 (Np-3) | -117 ± 3.7 (Np-6) | -100.5 ± 2.7 (Np-6) | -120.1 ± 4.5 (Np-3) |

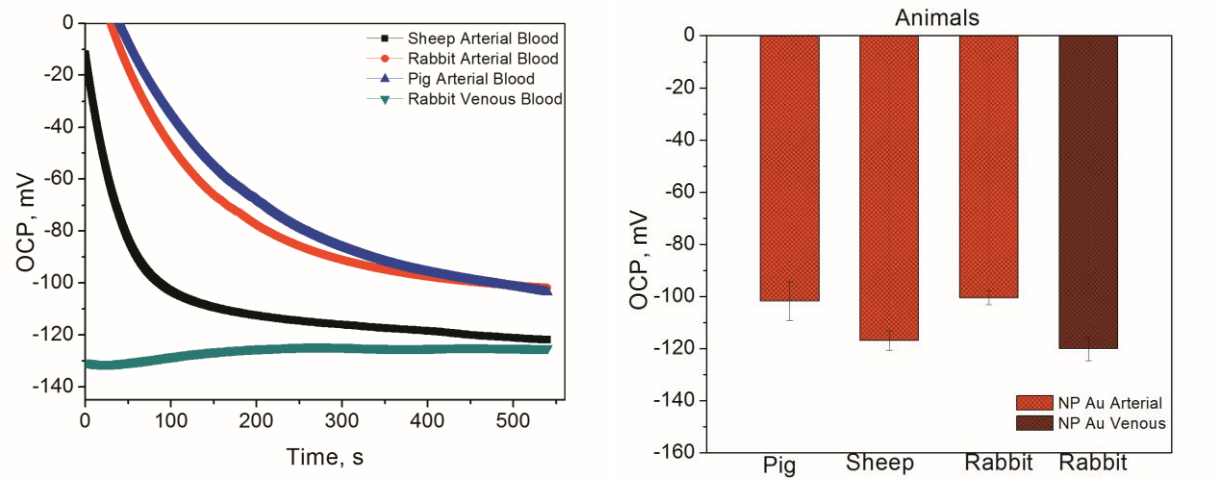


**Figure 3.16** OCP in mV of nanoporous gold in different animals: Sheep, Pig arterial blood, Rabbit arterial and venous blood. Right bar graph shows OCP of nanoporous gold in different animals: Sheep, Pig arterial blood, Rabbit arterial and venous blood. Error bars represent the standard deviations obtained from 3 electrodes.

### 3.14 OCP of healthy human volunteers

To obtain the average OCP of human blood, fresh blood was collected from 49 Healthy volunteers (20 Male, 26 Female, and 3 didn't report) and OCP measurements were made using a nanoporous gold electrodes (60% of the electrodes were light) and Ag/AgCl electrode connected to an Autolab potentiostat, which is able to measure the OCP of three electrodes at the same time. The electrodes were immersed in blood samples and OCP was recorded for ~10 minutes. Along with OCP, blood gas values ($PCO_2$ & $PO_2$) and lactate, glucose, and chloride were measured. $PCO_2$ and $PO_2$ and lactate, glucose, chloride were measured using radiometer. $PCO_2$ is partial pressure of carbon dioxide dissolved in blood and $PO_2$ is partial pressure of oxygen dissolved in blood. Table 3.8 shows the values obtained for the 49 volunteers. Attempts were made to determine if there was a correlation between OCP and $PCO_2$ or $PO_2$. As can be seen

in Figure 3.17, plots of $PCO_2$ Vs OCP and $PO_2$ Vs OCP gave no correlation. There is also no significant difference in the OCP between male (OCP =-113.9±14.9) and female (OCP = -114.5±16.8). The average OCP of Human blood from the data is (-114.2±15.2)

**Table 3.8** OCP, $PCO_2$, $PO_2$, glucose, lactate, chloride of 49 healthy human volunteers.

| Volunteer | Sex | OCP, mV | $PCO_2$ (mm/Hg) | $PO_2$ (mm/Hg) | Glucose (mmol/L) | Lactate (mmol/L) | Chloride (mmol/L) |
|---|---|---|---|---|---|---|---|
| 1 | Female | -101 | 38.8 | 35.2 | 4.4 | 2.2 | 110 |
| 2 | Female | -122 | 50.1 | 37.7 | 5.1 | 1.4 | 107 |
| 3 | Female | -159 | 52.9 | 28.3 | 5 | 2.4 | 108 |
| 4 | Male | -103 | 40.6 | 87.1 | 5 | 1.6 | 107 |
| 5 | Female | -108 | 45.1 | 47.1 | 5.2 | 1.3 | 107 |
| 6 | Male | -139 | 48.8 | 45.7 | 4 | 1.8 | 102 |
| 7 | Female | -122 | 59.2 | 26 | 4.4 | 1.6 | 106 |
| 8 | Male | -136 | 54.5 | 34.8 | 6.8 | 2.4 | 101 |
| 9 | Female | -123 | 46.6 | 51.3 | 4.8 | 2.1 | 105 |
| 10 | Male | -127 | 48.4 | 46.8 | 6.7 | 1.9 | 103 |
| 11 | Female | -121 | 54.2 | 28.4 | 4.4 | 1.3 | 101 |
| 12 | Female | -121 | 52.9 | 28.3 | 4.7 | 2.1 | 105 |
| 13 | Female | -114 | 51.1 | 32.4 | 4.5 | 1.6 | 106 |
| 14 | Female | -126 | 46.9 | 33.3 | 4.4 | 1.6 | 103 |
| 15 | Male | -79 | 63.2 | 28 | 4.9 | 1.8 | 102 |
| 16 | Male | -110 | 8.5 | 41.5 | 4.2 | 1.9 | 101 |
| 17 | Female | -119 | 33.4 | 138 | 4.5 | 2 | 107 |
| 18 | Male | -101 | 44 | 44.3 | 5.2 | 1.8 | 106 |
| 19 | Male | -121 | 55.1 | 46.4 | 3.9 | 1.8 | 104 |
| 20 | Female | -85 | 40.6 | 52.5 | 7.2 | 2.2 | 107 |
| 21 | Male | -117 | 48.8 | 53.8 | 6.3 | 1.8 | 104 |
| 22 | Male | -121 | 51.2 | 39.8 | 5.8 | 1.5 | 102 |
| 23 | Male | -129 | 63.1 | 29.4 | 6.4 | 2.1 | 102 |
| 24 | Female | -124 | 55.8 | 26.1 | 7.2 | 2.2 | 104 |
| 25 | Female | -120 | 50.2 | 38.6 | 4.6 | 2.9 | 105 |
| 26 | Female | -112 | 53.4 | 46 | 4.7 | 1.8 | 103 |
| 27 | Female | -114 | 45.8 | 98.3 | 6.8 | 1.4 | 107 |
| 28 | Female | -131 | 54.4 | 35.7 | 5.5 | 2.4 | 99 |
| 29 | Male | -108 | 58.8 | 22.7 | - | - | 104 |
| 30 | Male | -114 | 55.6 | 28.2 | 4.2 | - | 103 |
| 31 | Female | -116 | 53.3 | 25.6 | 4 | 1.9 | 105 |

| | | | | | | | |
|---|---|---|---|---|---|---|---|
| 32 | Male | -101 | 50.1 | 60.1 | 4.8 | 2 | 106 |
| 33 | Female | -113 | 51.9 | 44.5 | 4.4 | 2.6 | 108 |
| 34 | Male | -115 | 63.2 | 34 | 3.2 | 2.7 | 103 |
| 35 | Male | -91 | 53.5 | 43.2 | 5.2 | 2.7 | 101 |
| 36 | Male | -114 | 59.2 | 25.2 | 5 | 2.5 | 102 |
| 37 | Female | -64 | 59.9 | 24.2 | 5.4 | 3.4 | 100 |
| 38 | Female | -122 | 45.7 | 27.9 | 8.5 | 2.1 | 103 |
| 39 | Female | -108 | 39.1 | 46.3 | 10.1 | 4.4 | 107 |
| 40 | Female | -106 | 53.5 | 23.2 | 4.5 | 1.9 | 105 |
| 41 | Female | -118 | 49.2 | 35.1 | 6.6 | 2.1 | 102 |
| 42 | Male | -102 | 53.1 | 32 | 5.6 | 1.7 | 100 |
| 43 | Female | -112 | 58.4 | 30 | 4.4 | 1.9 | 104 |
| 44 | Female | -95 | 37.1 | 83.2 | 8.3 | 1.8 | 106 |
| 45 | - | -122 | 52 | 34.7 | 5.4 | 1.2 | 104 |
| 46 | - | -125 | 44.8 | 36.3 | 4.9 | 0.9 | 107 |
| 47 | - | -114 | 46.8 | 80.5 | 5.2 | 1.2 | 105 |
| 48 | Male | -124 | 49.3 | 40.1 | 4.4 | 1.8 | 106 |
| 49 | Male | -125 | 48 | 55.7 | 4.9 | 1 | 104 |

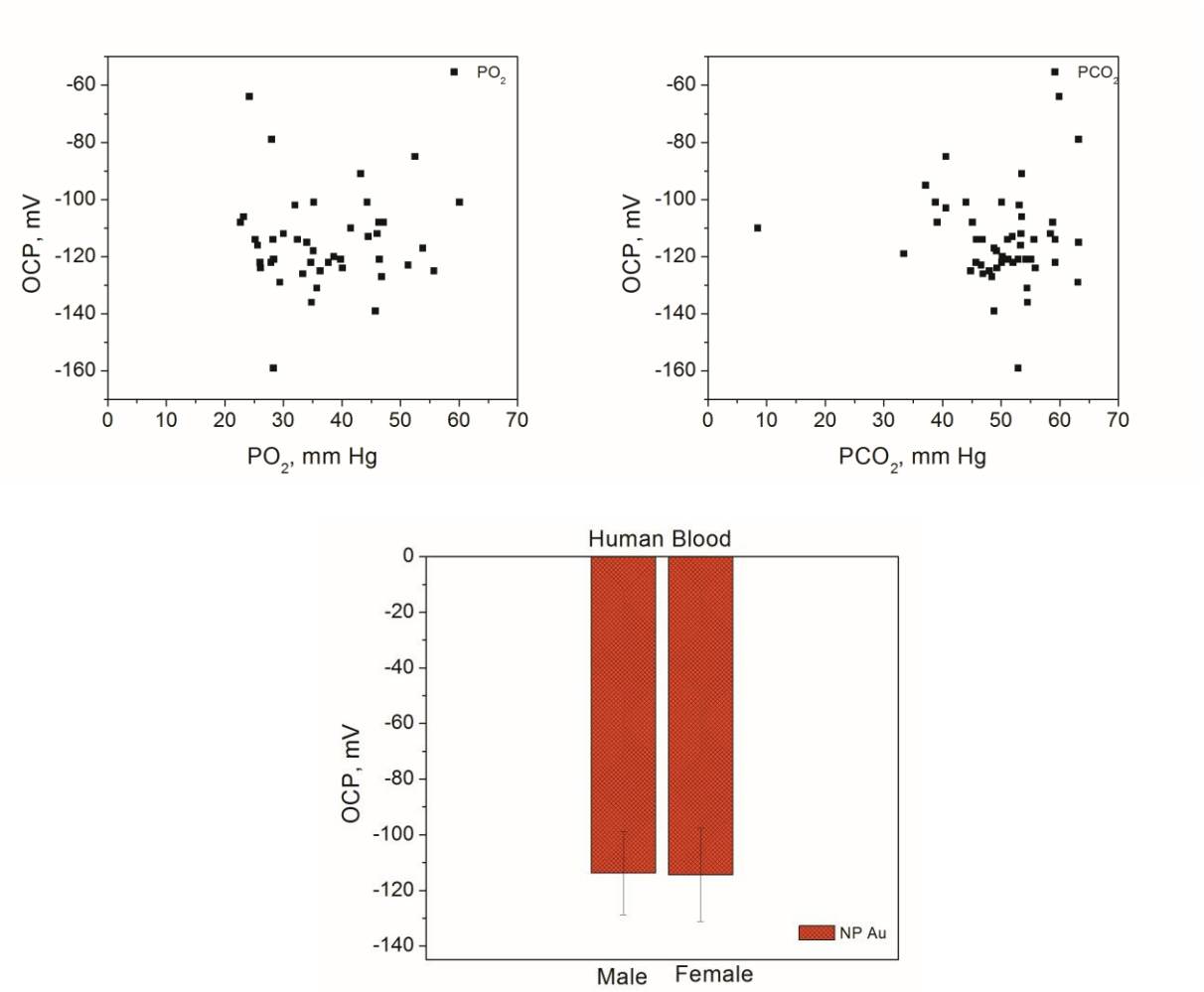


**Figure 3.17** OCP of healthy humans. (A) plot of OCP Vs $PCO_2$ (B) plot of OCP Vs $PO_2$ (C) OCP of male and female

### 3.15 Addition of Ascorbic Acid to Rabbit blood and measurement of OCP

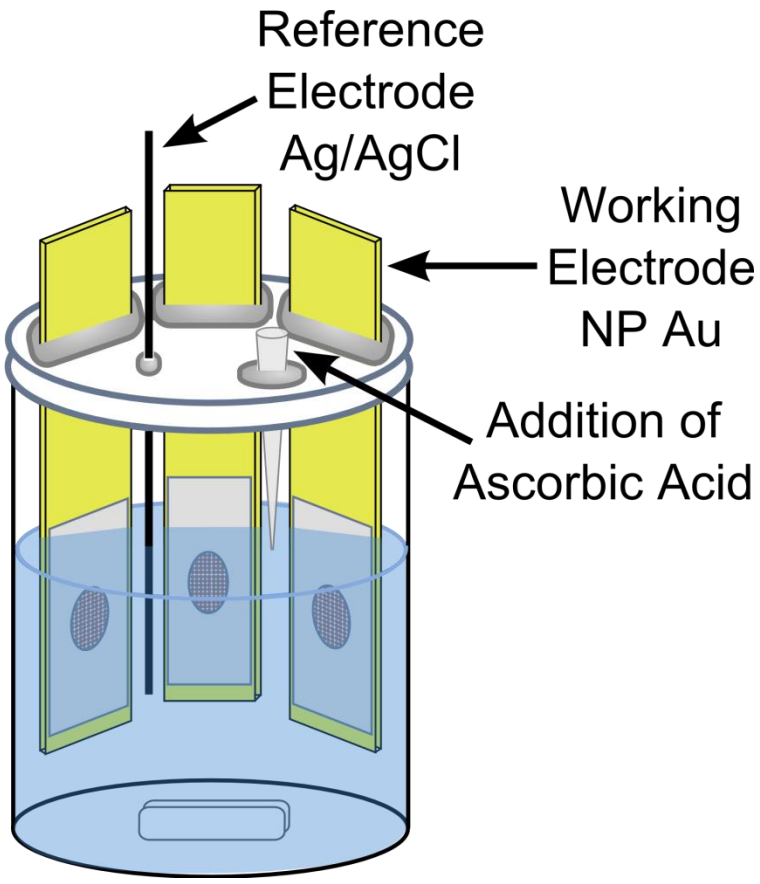


**Figure 3.18** A three electrode electrochemical setup for the measurement of OCP before and after the addition of ascorbic acid.

Rabbit blood was collected and the OCP at three nanoporous electrodes was measured simultaneously using the Autolab potentiostat. Figure 3.18 shows the electrochemical setup measuring OCP and addition of ascorbic acid. The advantage of this potentiostat is we can run OCP for three electrodes at a same time in a single sample of blood. Ascorbic Acid, 6 mM (reducing agent) was added after nine minutes and stir the solution until it reaches steady state, the potential dropped as observed in Figure 3.19. In Table 3.9, the OCP of nanoporous gold and planar gold in sheep blood before and after addition of ascorbic acid (AA) are shown. The difference in the OCP

immediately before and after addition of ascorbic acid is indicated as ΔE. Nanoporous gold electrodes showed a greater change in the OCP compared to planar gold electrodes.

**Table 3.9** OCP of nanoporous gold (Dark colored) and planar gold in sheep blood before and after addition of ascorbic acid 2mM (AA)

| | V before addition of AA ( ~9 min) | Final after addition of AA | ΔE mV | Average | Std dev |
|---|---|---|---|---|---|
| **NP1** | -0.099 | -0.141 | 42.3 | | |
| **NP2** | -0.101 | -0.143 | 41.6 | | |
| **NP3** | -0.104 | -0.135 | 30.2 | | |
| **NP4** | -0.099 | -0.135 | 35.8 | | |
| **NP5** | -0.097 | -0.131 | 34.4 | 36.9 | 5.1 |
| **Planar 1** | -0.153 | -0.19 | 37 | | |
| **Planar 2** | -0.158 | -0.188 | 29.1 | | |
| **Planar 3** | -0.167 | -0.19 | 22.8 | | |
| **Planar 4** | -0.166 | -0.19 | 23.8 | 29.4 | 6.3 |

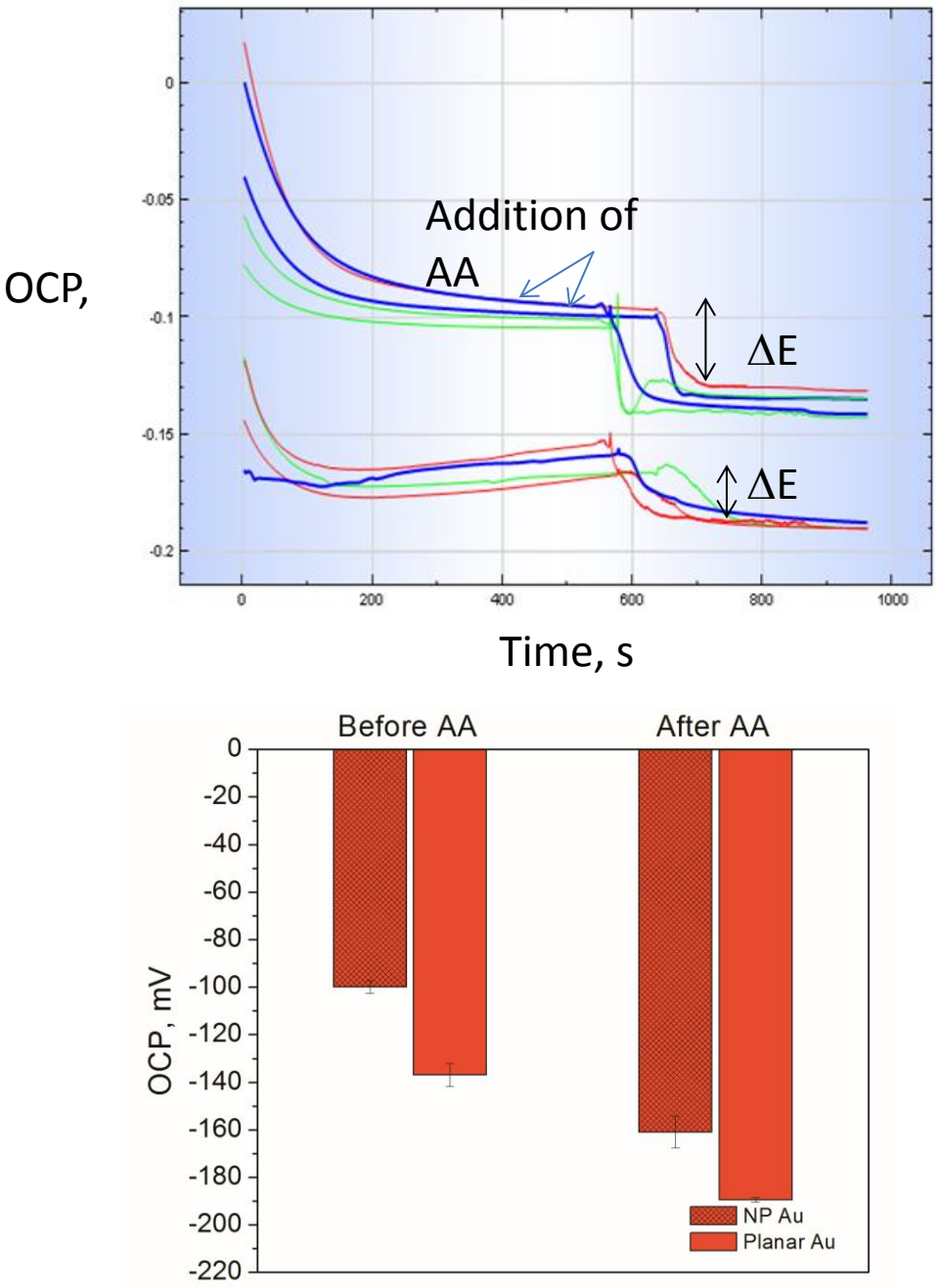


**Figure 3.19** OCP of nanoporous gold in Rabbit blood before and after the addition of ascorbic acid after ~ 9 minutes. The lower bar graph shows the OCP of nanoporous gold in Rabbit blood and the difference in potential before and after the addition of ascorbic acid (2mM). Error bars represent the standard deviations obtained from 4-5 electrodes.

### 3.16 Addition of Ascorbic acid to Sheep blood.

Sheep blood was collected and the OCP was measured using a CH instrument potentiostat, one electrode at a time. Ascorbic Acid, 5 mM (reducing agent) was added after nine minutes to sheep blood (1.5 mL). This results in a drop in potential as can be seen in Figure 3.20. After the potential stabilized, an additional aliquot of ascorbic acid was added. In the same way, a total of six consecutive additions of ascorbic acid were added in regular intervals to the blood sample. Figure 3.20 shows clearly the additions of ascorbic acid at different intervals. The difference in the OCP before and after addition of ascorbic acid is indicated as ΔE. Figure 3.20, 3.21 & 3.22 show the plot of concentration of ascorbic acid Vs ΔE in sheep blood and PBS 7.0. As the concentration of ascorbic acid increased, the OCP became more negative. It clearly shows nanoporous electrodes respond to the addition of reduced species to blood. Figure 3.23 shows CV of sheep blood after addition of ascorbic acid. The peak at 0.1 V corresponds to the oxidation of ascorbic acid.

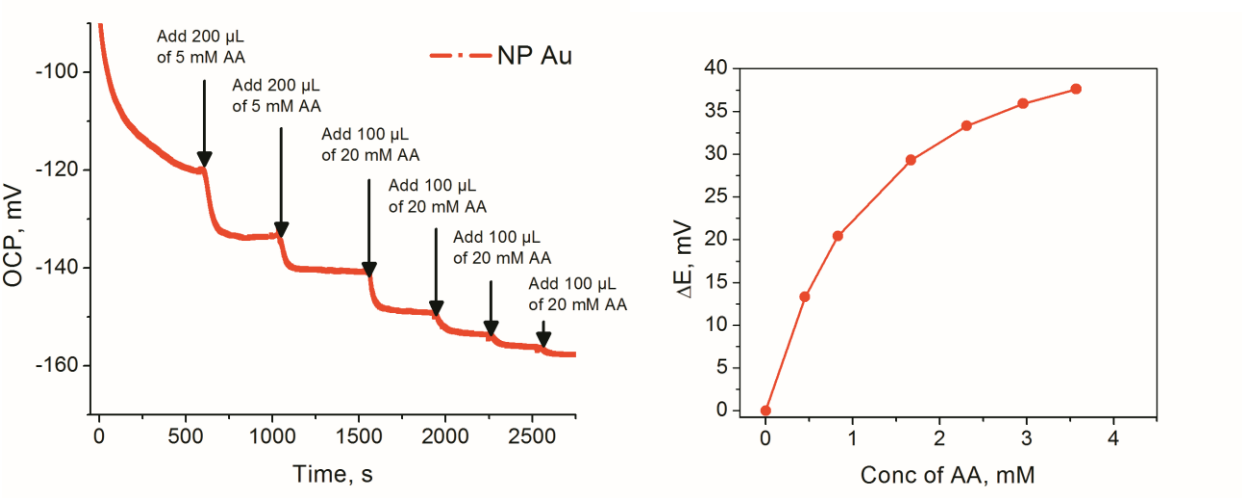


**Figure 3.20.** The change in OCP upon addition of ascorbic acid to blood in different intervals of time. Right graph shows plot of ΔE Vs concentration of ascorbic acid added.

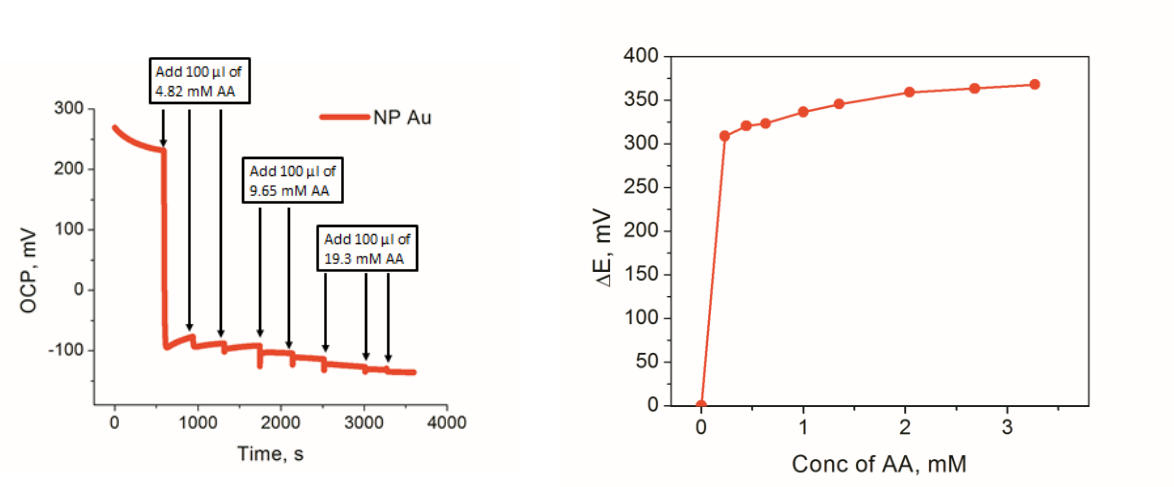


**Figure 3.21.** The change in OCP upon addition of ascorbic acid in in 0.1 M Phosphate buffer (pH 7)/0.1 M KCl at different intervals of time. Right graph shows plot of ΔE (V) vs concentration of ascorbic acid added to solution.

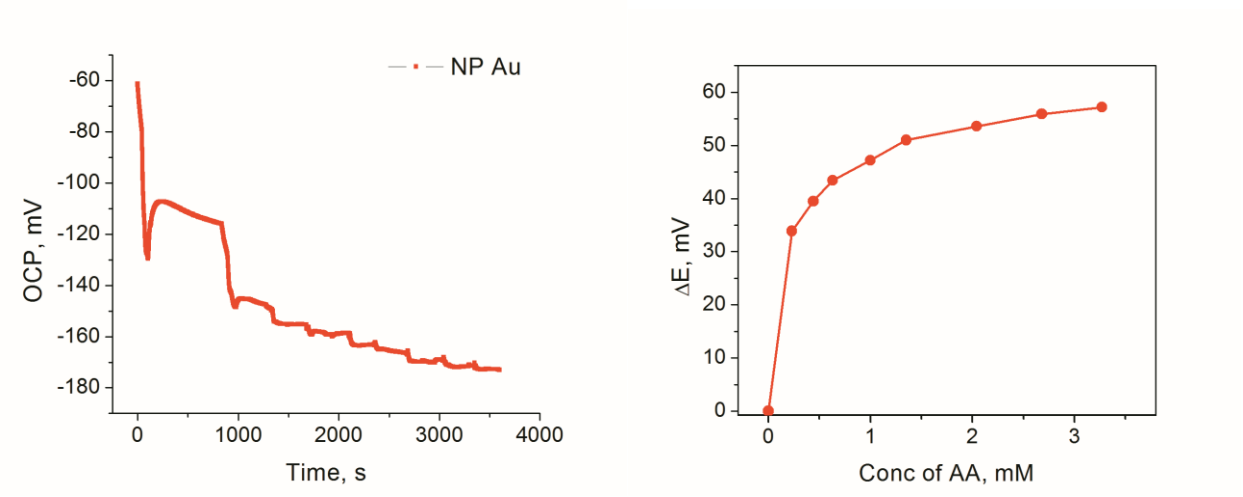


**Figure 3.22.** The change in OCP upon addition of ascorbic acid to Sheep blood at different intervals of time. Right graph shows plot of ΔE Vs concentration of ascorbic acid added to solution.

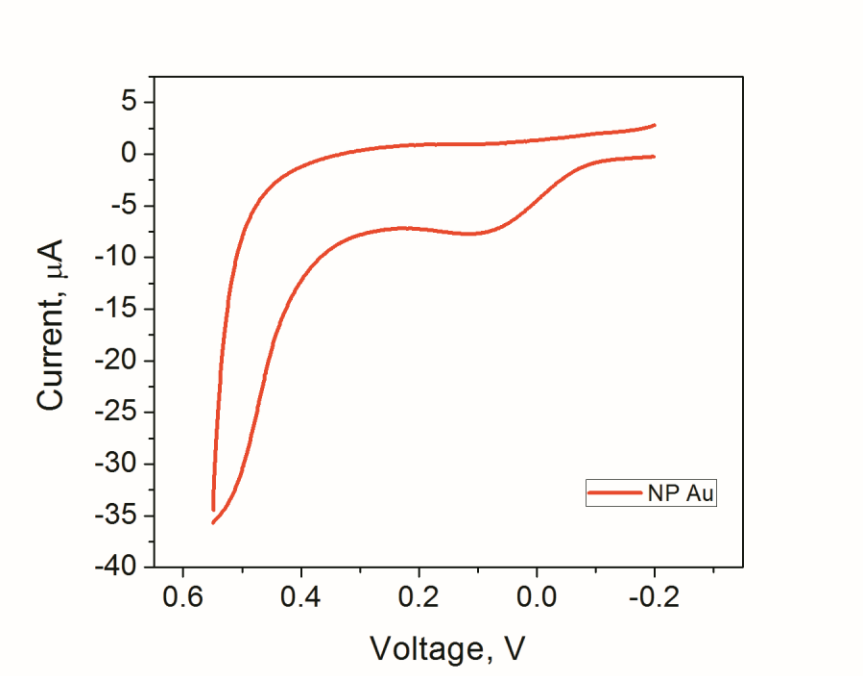


**Figure 3.23.** Cyclic voltammetric curve of in Sheep blood after addition of ascorbic acid (2mM) at scan rate 100 mV/s.

# Summary

Nanoporous gold was prepared by the chemical dealloying of a Ag:Au alloy at different times. The effect of protein adsorption on nanoporous gold immersed in biofouling solutions was studied. In this work, we have shown that electrochemical measurements can be made using nanoporous gold even in high concentrations of biofouling agents such as albumin. We have also shown that nanoporous gold can be successfully used to measure the redox potential of blood and plasma. Nanoporous gold electrodes have many advantages due to their higher surface area and porosity.

Fabrication of nanoporous gold was done by dealloying a Ag/Au alloy in nitric acid, which removes the silver resulting in a highly porous structure of gold. The dealloying time in concentrated nitric acid is an important factor in that it controls the porosity of the electrode and its surface area. After the preparation of nanoporous gold, the electrode with highest surface was taken and the electrochemical response in the presence of biofouling agents like bovine serum albumin was studied. The response at nanoporous gold electrodes were compared to planar gold electrodes. After immersing nanoporous gold electrodes and planar gold electrodes in a buffered solution containing potassium ferricyanide and bovine serum albumin, immediate reduction in Faradaic peak current and increase in peak splitting was seen for planar gold electrodes. In

contrast, nanoporous gold electrodes showed no such changes and they retained their electrochemical activity in presence of biofouling solutions. The redox activity of potassium ferricyainde at nanoporous gold was retained serum and blood as well. Nanoporous gold having 3D network of small nanometer sized pores and ligaments are believed to impede the transport of large biomolecules while allowing small redox molecules to exchange electrons effectively with the electrode.

While exploiting the nanoscale features of the electrode surface, electrochemical measurements in real blood and serum was undertaken. The open circuit potential (e.g., redox potential) of blood and plasma of various animals like Pig, Rabbit, Rat, Monkey and Humans were measured using nanoporous gold. The redox potential was compared to values obtained at planar gold. Both redox potential values were different from each other and there was animal-to-animal variability due to the different constituents present in blood and plasma. The redox potential of healthy rabbit blood and crashed rabbit blood was measured and the values were found to be different from each other indicating that redox potential is sensitive to the animal condition. The redox potential of human blood was also measured and it showed same value for both male and female. Upon addition of a reducing agent (ascorbic acid) to rabbit and sheep blood, the change in potential ($\Delta E$) for nanoporous gold was found to be higher compared to flat gold. Overall, nanoporous gold electrodes have showed better electrochemical performance in biologic solutions than planar gold.

# Future work

Future work should focus on improving the properties of nanoporous gold such as increasing the surface area and maintaining small pore size. Increasing the surface area of nanoporous gold will increase the number of sites for electron transfer and ideal surface topography should be designed to decrease the effective distance for the electron transfer between electrode and redox active group in a biomolecule. Nanoporous gold having small pores and a high roughness factor will strongly influence protein adsorption. Having small pores will stop larger proteins from entering inner surfaces and ideally facilitate electron transfer with smaller redox species in biological media. Nanoporous gold prepared by dealloying Au: Ag alloy has ~ 10% of silver, which is showing a retained electrochemical activity in biological media. The dealloying time should be standardized to achieve electrodes with similar porosity, surface area, and percent silver. EDX and XPS can be used to evaluate the silver composition at different dealloying time intervals while SEM images can help show the structure and morphological changes as a function of dealloying time. Nanoporous gold electrodes can be further evaluated using transmission electron microscopy (TEM) to know the three-dimensional (3D) structure, an ideal way to see the inner pore network and can quantitatively evaluate the average diameter of the ligaments and nanopore channels.

Further OCP and electrochemical measurements can be made for biomolecules like glutathione peroxidase, catalase, cysteine, lactate, pyruvate, uric acid and NADH. Redox status in humans is maintained within a narrow range and can be altered during critical illness and injury. There exists a complex relationship between the redox state of blood and survival during critical illness and injury, so monitoring redox chemistry during critical illness for humans should be carried out. Because the OCP of stored pig blood varied after 2 days, it would be worth studying the OCP of stored human blood products.

# References


1. Glomm, W. R.; Halskau.; Hanneseth, A. D.; Volden, S. Adsorption Behavior of Acidic and Basic Proteins onto Citrate-Coated Au Surfaces Correlated to Their Native Fold, Stability, and pI *The Journal of Physical Chemistry B* **2007***, 111*, 14329-14345.

2. Patel, J.; Radhakrishnan, L.; Zhao, B.; Uppalapati, B.; Daniels, R. C.; Ward, K. R.; Collinson, M. M. Electrochemical Properties of Nanostructured Porous Gold Electrodes in Biofouling Solutions *Anal. Chem.* **2013***, 85*, 11610-11618.

3. Heli, H.; Sattarahmady, N.; Jabbari, A.; Moosavi-Movahedi, A. A.; Hakimelahi, G. H.; Tsai, F. Adsorption of human serum albumin onto glassy carbon surface – Applied to albumin-modified electrode: Mode of protein–ligand interactions *J Electroanal Chem* **2007***, 610*, 67-74.

4. Moulton, S. E.; Barisci, J. N.; Bath, A.; Stella, R.; Wallace, G. G. Studies of double layer capacitance and electron transfer at a gold electrode exposed to protein solutions *Electrochim. Acta* **2004***, 49*, 4223-4230.

5. Moulton, S. E.; Barisci, J. N.; Bath, A.; Stella, R.; Wallace, G. G. Studies of double layer capacitance and electron transfer at a gold electrode exposed to protein solutions *Electrochim. Acta* **2004***, 49*, 4223-4230.

6. Moulton, S. E.; Barisci, J. N.; Bath, A.; Stella, R.; Wallace, G. G. Investigation of protein adsorption and electrochemical behavior at a gold electrode *J. Colloid Interface Sci.* **2003***, 261*, 312-319.

7. Moulton, S. E.; Barisci, J. N.; Bath, A.; Stella, R.; Wallace, G. G. Investigation of protein adsorption and electrochemical behavior at a gold electrode *J. Colloid Interface Sci.* **2003***, 261*, 312-319.

8. Ying, P.; Viana, A. S.; Abrantes, L. M.; Jin, G. Adsorption of human serum albumin onto gold: a combined electrochemical and ellipsometric study *J. Colloid Interface Sci.* **2004***, 279*, 95-99.

9. AnonymousAllen J. Bard and Larry R. Faulkner, Electrochemical Methods: Fundamentals and Applications, New York: Wiley, 2001, 2nd ed. *Russian J. Electrochem.* **2002***, 38*, 1364-1365.

10. Bar-Or, D.; Bar-Or, R. Measurement and uses of oxidative status. **2013**.

11. Sean, B.; Fred, H.; L, L. K.; C, R. M.; Kevin, W. Non-biofouling, universal redox electrode and measurement system. **2007**.

12. Rael, L. T.; Bar-Or, D.; Bar-Or, R. Method and apparatus for measuring oxidation-reduction potential. **2014**.

13. Nordstrom, D. K. Thermochemical redox equilibria of ZoBell's solution *Geochim. Cosmochim. Acta* **1977***, 41*, 1835-1841.